Universidade de Aveiro

2022

ALEXANDRE DAVID DE AMORIM GONÇALVES

FUNÇÃO DAS COPINE-1 E COPINE-3 NA RESPOSTA DE CÉLULAS EPITELIAIS A DANOS NA MEMBRNA PLASMÁTICA INDUZIDOS PELA PNEUMOLISINA

ROLE OF COPINE-1 AND COPINE-3 IN THE EPITHELIAL CELL RESPONSE TO PNEUMOLYSIN-INDUCED PLASMA MEMBRANE DAMAGE

Universidade de Aveiro

2022

ALEXANDRE DAVID DE AMORIM GONÇALVES

FUNÇÃO DAS COPINE-1 E COPINE-3 NA RESPOSTA DE CÉLULAS EPITELIAIS A DANOS NA MEMBRNA PLASMÁTICA INDUZIDOS PELA PNEUMOLISINA

ROLE OF COPINE-1 AND COPINE-3 IN THE EPITHELIAL CELL RESPONSE TO PNEUMOLYSIN-INDUCED PLASMA MEMBRANE DAMAGE

Dissertação apresentada à Universidade de Aveiro para cumprimento dos requisitos necessários à obtenção do grau de Mestre em Biologia Molecular e Celular, realizada sob a orientação científica da Doutora Sandra Manuela Rodrigues Sousa Cabanes, investigadora principal do grupo de *Cell Biology of Bacterial Infections* do Instituto de Investigação e Inovação em Saúde (i3S), e sob a coorientação do Professor Artur Jorge da Costa Peixoto Alves, Professor Auxiliar com agregação do Departamento de Biologia da Universidade de Aveiro.

Dedico este trabalho aos meus familiares, namorada e amigos pelo constante apoio.

o júri

Presidente:	Professor Doutor António José de Brito Fonseca Mendes Calado, Professor Auxiliar, Departamento de Biologia, Universidade de Aveiro
Vogal – Arguente	Doutora Sílvia Marisa Nogueira do Vale Costa, Investigadora Júnior, Instituto Gulbenkian de Ciência
Vogal – Orientadora	Doutora Sandra Manuela Rodrigues Sousa Cabanes, Investigadora Principal, i3S – Instituto de Investigação e Inovação em Saúde, Universidade do Porto

agradecimentos

A realização deste trabalho nunca teria sido possível sem a ajuda e o apoio dos outros. Assim sendo, desejo expressar os meus mais sinceros agradecimentos aos que me permitirem concluir esta dissertação.
À Dra. Sandra Sousa, pela confiança e pela oportunidade que me deu de poder realizar a minha dissertação de mestrado no seu laboratório do CBBI. Pela sua orientação, disponibilidade, conselhos e ensinamentos que me foi transmitindo ao longo do estágio. Aos meus colegas do laboratório do CBBI e GM2, que se tornaram amigos, pela vossa companhia, partilhas de experiência e gargalhadas, mas principalmente à Joana Pereira, que me acompanhou sempre, a qualquer momento ou hora, que me ajudou tanto na parte laboratorial como durante as análises, que me apoiou nos momentos de maior stress, que sempre me motivou e confiou em mim.
Ao professor e coorientador Dr. Artur Alves, pelo esclarecimento de dúvidas, e acompanhamento.
Por último, quero agradecer aos meus pais, irmãs, amigos e em especial à Mariana, pelo vosso apoio incansável ao longo desta etapa.

palavras-chave

integridade da membrana plasmática, toxinas formadoras de poros, copine, permeabilização celular, intoxicação, *Streptococcus pneumoniae*, pneumolisina

resumo

A formação da membrana plasmática foi essencial para o desenvolvimento da Vida e para o processo de Evolução. A membrana plasmática é a primeira barreira protetora da célula. Devido ao seu papel crucial na sobrevivência celular, bactérias patogénicas humanas produziram toxinas formadoras de poros capazes de permeabilizar a membrana plasmática através da formação de poros estáveis. A formação de poros resulta na alteração da permeabilidade da membrana, permitindo assim trocas descontroladas de iões, tais como cálcio, e de pequenas moléculas entre o meio intracelular e extracelular, o que pode resultar na morte celular. Para superar os danos causados, as células desenvolveram mecanismos de reparação que promovem a sobrevivência celular. Um destes mecanismos de reparação baseia-se na libertação de vesículas extracelulares que permitem a eliminação de poros da superfície celular. A análise proteómica de vesículas libertadas por células intoxicadas revelou um enriquecimento de copine-1 e copine-3, levantando a hipótese que estas proteínas estão potencialmente envolvidas na reparação de danos na membrana plasmática.

A copine-1 e a copine-3 são proteínas citoplasmáticas que respondem ao cálcio, isto é, são capazes de translocarem para a membrana plasmática em resposta a um aumento intracelular dos níveis de cálcio. Evidências experimentais indicam que a copine-1 e a copine-3 estão envolvidas na reparação de danos induzidos por toxinas. No presente trabalho, pretendemos avaliar o papel destas proteínas em resposta às toxinas bacterianas formadoras de poros, como a pneumolisina, seguindo duas abordagens: a avaliação da capacidade de células que não expressam copine-1 ou copine-3 de recuperarem a integridade da sua membrana plasmática após intoxicação e a avaliação da localização intracelular das copine-1 e copine-3 em células intoxicadas.

Observámos que células que não expressam as copine-1 e copine-3 não são capazes de reparar os danos causados pelas toxinas na membrana plasmática e não recuperam a integridade da mesma. A copine-1 e a copine-3 são, portanto, essenciais para a recuperação da integridade da membrana após intoxicação. Observámos ainda que durante a intoxicação, a copine-1 e a copine-3 são especificamente recrutadas para o córtex celular, onde acumulam com maquinarias de reparação já caraterizadas.

Ensaios adicionais devem ser realizados para descobrir o papel molecular e os parceiros de interação das copine-1 e copine-3 na reparação dos danos na membrana plasmática.

keywords

plasma membrane integrity, pore-forming toxins, copine, cell permeabilization, intoxication, *Streptococcus pneumoniae*, pneumolysin

abstract

The establishment of the plasma membrane was essential in the development of Life and evolution, it acts as the first protective barrier of cells. Due to its crucial importance to ensure cell survival, human bacterial pathogens produce pore-forming toxins able to permeabilize the plasma membrane, forming stable protein pores. The formation of the pores alters the membrane permeability allowing uncontrolled exchanges of ions, such as calcium and potassium, and small molecules between the intracellular and extracellular milieus, which can ultimately lead to cell death. Cells have, thus, developed several repair mechanisms to overcome the damage, and promote cell survival. One of these repair mechanisms relies on the release of extracellular vesicles that extrude the pores from the cell surface. Proteomic analysis of vesicles released by intoxicated cells revealed the enrichment of copine-1 and copine-3, and raised the hypothesis that these proteins are potentially involved in the repair of plasma membrane damage.

Copine-1 and copine-3 are cytoplasmic calcium-responsive proteins able to translocate to the plasma membrane in response to an increase in intracellular calcium levels. Experimental evidence points out that copine-1 and copine-3 have a role in the repair of toxin-induced damage. Here we aimed to assess the role of these proteins in response to bacterial pore-forming toxins, such as pneumolysin, by two complementary approaches: evaluating the ability of cells depleted for the expression of copine-1 or copine-3 to recover their plasma membrane integrity upon intoxication and assessing the intracellular localization of copine-1 and copine-3 in intoxicated cells.

We found that cells that do not express copine-1 or copine-3 are not able to repair plasma membrane damage induced by toxins and do not recover their plasma membrane integrity. Copine-1 and copine-3 are thus essential for the recovery of membrane integrity after intoxication. We also observed that, upon intoxication, copine-1 or copine-3 are specifically recruited to the cortex of the cell, where it accumulates with already characterized repair machinery.

Further assays should be performed to uncover the molecular role and the interaction partners of copine-1 and copine-3 in the repair of plasma membrane damage.

Table of contents

List of Tables

List of Figures

Abbreviations and terms

AIF	Apoptosis-inducing factors;
ALO	Anthrolysin O;
ATP	Adenosine triphosphate;
BBB	Blood Brain Barrier;
CBBI	Cell Biology of Bacterial Infections;
CDCs	Cholesterol-dependent cytolysins;
CPNE1	Copine-1;
CPNE3	Copine-3;
CRISPR repeats;	Clustered regularly interspaced short palindromic
DMEM	Dulbecco's Modified Eagle Medium;
DPBS	Dulbecco's Phosphate Buffered Saline 1x;
ECL	Enhanced Chemiluminescence;
ESCRT	Endosomal sorting complex required for transport:
EVs	Extracellular vesicles;
FBS	Fetal Bovine Serum;
FSC-A	Forward Scatter Area;
FSC-H	Forward Scatter Height;
gDNA	Genomic DNA;
GFP	Green fluorescent protein;
GPI	Glycosylphosphatidylinositol;
HBSS	Hank's Balanced Salt Solution;
Hlg	γ-hemolysin;
HlyE	Haemolysin E;
HRP	Horseradish Peroxidase;
IL-8	Interleukin 8;
KO	Knockout;
KO *CPNE1*	Knockout for copine-1;

KO *CPNE3*	Knockout for copine-3;
LB	Luria-Bertani;
LLO	Listeriolysin O;
MAPK	Mitogen-activated protein kinase;
MEK1	Mitogen-activated protein kinase/extracellular signal-regulated kinase kinase;
MLKL	Mixed lineage kinase domain-like protein;
mtDNA	Mitochondrial DNA
MW	Molecular weight;
NI	Non-intoxicated;
NLRP3	Nod-like receptor family pyrin domain-containing 3;
NMHCIIA	Non-muscle heavy chain of myosin IIA;
NT	Non-transfected;
p38/MAPK	Mitogen-activated protein kinases p38;
PFO	Perfringolysin O;
PFPs	Pore-forming proteins;
PFTs	Pore-forming toxins;
PI	Propidium iodide;
PLP1	Perforin like proteins 1;
PLY	Pneumolysin;
PM	Plasma membrane;
PP5	Protein phosphatase 5;
ROS	Reactive oxygen species;
SEM	Standard error of the mean;
SLO	Streptolysin O;
SSC-A	Side Scatter Area;
UPR	Unfolded protein response;
vWA	von Willerbrand factor A-domain;
WHO	World Health Organization;
WT	Wild-type.

CHAPTER 1

Introduction

1.1 – Importance of the plasma membrane

Among the numerous constituents of the cell, the plasma membrane (PM) is considered a major pillar in the long story of life. Its formation was a key event in the establishment of Life and in evolution (Deamer *et al*., 2002). The function of the PM is not limited to the separation of the extracellular from the intracellular space but it also relates to the establishment of gradients and the maintenance of specific chemical compositions and/or properties in the intracellular environment (Bischofberger *et al*., 2012; Iacovache *et al*., 2008). The plasma membrane is the first protective barrier of cells and thus, its integrity is essential to maintain cellular homeostasis and to ensure cell survival (Brito *et al*., 2019a; Los *et al*., 2013).

PM disruptions often occur in healthy conditions, particularly in mechanically active tissues, such as cells of the aorta, muscle, gut and skin, that are exposed to mechanical stress and high force constraints (Ammendolia *et al*., 2021; Dias & Nylandsted, 2021; McNeil, 1993). In addition, due to its critical importance for cell survival, the PM is an ideal target during external attacks such as infection by bacteria or virus. In particular, relevant human bacterial pathogens have developed pore-forming proteins (PFPs) that act by disrupting the PM integrity of host cells and disturbing cell signaling (Bischofberger *et al*., 2012; Brito *et al*., 2019a; Iacovache *et al*., 2008; Los *et al*., 2013). PFPs form pores in the cell PM, which dramatically alter membrane permeability allowing the uncontrolled exchanges between the extracellular and intracellular space, ultimately causing cell death and tissue destruction (Gilbert, 2002).

1.2 – Pore-forming proteins

PFPs are found in all kingdoms of life and have an extensive range of target cells. Even if their amino acid sequence is not conserved, they share the same overall mode of action. A great variety of higher organisms can produce PFPs, like parasites (PLP1) (Kafsack *et al*., 2009), mushrooms (pleurotolysin) (Tomita *et al*., 2004), plants (enterolobin)

(Sousa *et al*., 1994), animals such as sea anemone (equinatoxin II) (Kristan *et al*., 2009), and even mammals that use perforin as a part of their immune system to counter infection of microorganisms by killing infected or malignant cells (Voskoboinik *et al*., 2015).

1.3 – Bacterial pore-forming toxins: mechanisms of pore formation and role in infection

The biggest and best characterized class of PFPs is the family of bacterial pore-forming toxins (PFTs), which represent about 30 % of the reported cytotoxic bacterial proteins and are able to damage the PM of host cells by forming regular and stable pores in the PM lipid bilayer. PFTs contribute to the *in vivo* virulence and pathogenesis of bacteria, namely in humans (Dal Peraro & van der Goot, 2016; Los *et al*., 2013; Mondal *et al*., 2018; Verma & Chattopadhyay, 2021).

PFTs are classified based on the secondary structure that they adopt to penetrate the PM of the target cell. The region that perforates the PM, arranged in α-helices or β-barrels as the corresponding PFTs are referred to as α-PFTs and β-PFTs, respectively (Gouaux, 1997). α-PFTs and β-PFTs are both classified into different families (Table 1) defined by the toxins, their structure, their receptor binding, their mechanism of pore formation and the stoichiometry, and the diameter of the pore. α-PFTs are composed by the Colicin family, the Cytolisin A family and the Actinoporin family, while β-PFTs are composed by the Haemolysin family, the Aerolysin family and the cholesterol-dependent cytolysins (CDCs) family (reviewed by Dal Peraro & van der Goot, 2016).

Bacteria produce PFTs for many purposes and their effects are dependent on their concentration and activity (Pereira *et al*., 2022). At high doses (lytic concentrations), PFTs induce massive damage and kill host cells, to promote bacterial dissemination and disease progression. In particular, PFTs destroy human tight barriers and may directly kill cells from the immune system, thus annihilating both innate and adaptive immune responses (Verma et al., 2021). As examples, hemolysin A produced by *Escherichia coli* induces necrosis, apoptosis and inflammation on host immune cells and is associated with urinary tract infections and septicemia (Alouf, 2003; Czuprynski & Welch, 1995; Linhartová *et al*., 2010); listeriolysin O (LLO) produced by *Listeria monocytogenes* allows bacteria to escape from the internalization phagosomes contributing to intracytoplasmic growth and cell-to-cell spread avoiding immune cells surveillance (Hamon *et al*., 2012). *E. coli* also produces colicins, which are α-PFT that attacks other bacterial strains to reduce competition (Lakey *et al*., 1994). Pneumolysin (PLY) produced by *Streptococcus pneumoniae* targets alveolar

macrophages and neutrophils allowing pneumococcal proliferation in the lungs (Pereira *et al*., 2022). At sub-lytic concentrations, PFTs do not necessarily kill the cell but induce modifications of the cellular behavior and host physiology (Dal Peraro & van der Goot, 2016; Los *et al*., 2013). By allowing the free exchange of molecules between the intracellular and extracellular milieus, PFTs ensure nutrient availability for the bacteria as molecules such as amino acids, ions and ATP leak to the extracellular space.

Table 1: Classification of selected bacterial PFTs, their cellular receptors and associated pathogenesis. Reviewed and adapted from Bischofberger *et al*., 2012, Dal Peraro & van der Goot, 2016 and Los *et al*., 2013.

Species	PFT	Class	Family	Receptor	Associated pathogenesis
Escherichia coli	Colicin A	α	Colicins	Bacterial inner membrane or outer membrane	Competitive bacterial death
Escherichia coli	HlyE	α	Cytolisin A	Cholesterol	Diarrhea, hemorrhagic colitis, hemolytic-uremic syndrome
Staphylococcus aureus	Hlg	β	Haemolysins	Phosphatidylcholine	Skin infection, fatal sepsis, necrotizing fasciitis, pneumonia
Clostridium septicum	α-toxin	β	Aerolysin	GPI-anchored proteins	Enteric infections, wound infections, myonecrosis, necrotic enteritis
Bacillus anthracis	ALO	β	CDCs	Cholesterol	Anthrax, pulmonary infection, fatal systemic infections, respiratory failure
Clostridium perfringens	PFO	β	CDCs	Cholesterol	Myonecrosis, dysentery, enterotoxemia, enterocolitis
Listeria monocytogenes	LLO	β	CDCs	Cholesterol	Listeriosis, septicemia, meningoencephalitis, invasive neonatal infection
Streptococcus pneumoniae	PLY	β	CDCs	Cholesterol	Pneumonia, meningitis, otitis media, bacteremia
Streptococcus pyogenes	SLO	β	CDCs	Cholesterol	Skin infection, pharyngitis, rheumatic fever, necrotizing fasciitis, toxic-shock-like syndrome

ALO: Anthrolysin O; CDC: Cholesterol-dependent cytolysins; GPI: Glycosylphosphatidylinositol Hlg: γ-hemolysin; HlyE: Haemolysin E; LLO: Listeriolysin O; PFO: Perfringolysin O; PLY: Pneumolysin; SLO: Streptolysin O.

PFTs are secreted as monomeric water-soluble proteins that bind to a specific receptor expressed at the surface of target cells. Depending on the class of the PFT, these specific receptors can be lipids, sugars or proteins. The binding to specific receptors in the cell surface leads to an increase in the local concentration of PFTs favoring oligomerization, which is an important step for pore formation. For β-PFTs, oligomerization occurs at the surface of the cell membrane, leading to the assembly of a pre-pore that will later insert into the PM (Figure 1.A). In the case of α-PFTs, the oligomerization and the insertion of the PFT in the PM occurs simultaneously, which leads to the formation of partial or complete pores (Figure 1.B). In both cases, the oligomerization step results in a transmembrane and active pore, that disrupts the PM integrity of the host cell, and allows the entrance and exit of ions, small molecules or larger molecules, depending on the nature of the toxin and the size of pore (Bischofberger *et al*., 2012; Dal Peraro & van der Goot, 2016; Menestrina *et al*., 2001; Parker & Feil, 2005).

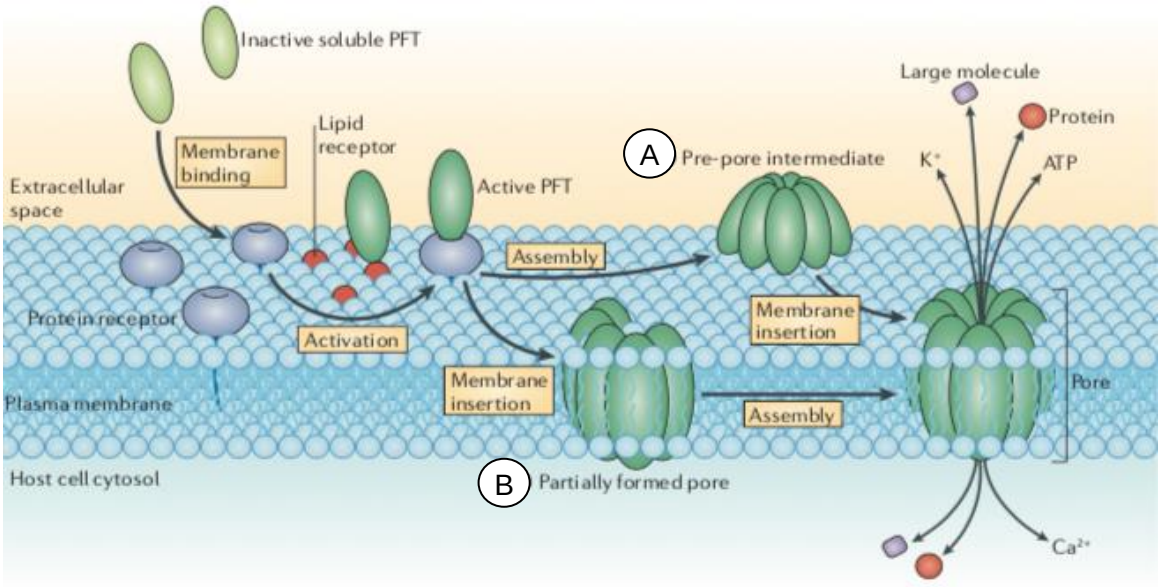

Figure 1: Schematic representation of the molecular mechanisms of pore formation by PFTs. Soluble PFTs bind to the protein receptors present at the surface of the PM, and toxin start to oligomerize following one of the two mechanisms. A: Pore formation pathway followed by most members of the β-PFTs group, where oligomerization occurs at the PM surface, forming a pre-pore that will continue its insertion into the membrane; B: Pore formation pathway followed by most members of the α-PFTs group, where the insertion of the PFT into the membrane occurs simultaneously to the oligomerization process, forming partially active pores. Reviewed and adapted from Dal Peraro & van der Goot, 2016.

During bacterial infection, PFTs trigger a variety of deleterious effects for the host,

such as inflammation, hijacking of host factors, programmed cell death and many others. Those effects vary according to the producer bacteria, the produced PFT, the biophysical properties of the pore, the exposure time, the site of infection and the distance between the infection foci and the target cell (Bischofberger *et al*., 2012; Gonzalez *et al*., 2008; Los *et al*., 2013). Among the many effects triggered by PFTs, two of them are common for almost every PFT. The first is the induction of PM dysfunction, which result in compromised integrity in both epithelial and endothelial barriers. The barrier dysfunction can be induced by PFTs in different ways, through direct attack of cells, or by hijacking the molecular pathways that regulate the extracellular matrix of the host cell. The impairment of epithelial barrier integrity allows bacteria, and their toxins, to access deeper tissues and to circulate in the host body, leading to bacteria dissemination. The second effect is the disruption of the host immune response. This disruption can occur in different manners. PFTs can directly kill immune cells or prevent their recruitment to the site of infection, thus supporting bacterial invasion and intracellular survival. In addition, PFTs can also hijack the host molecular defense pathways preventing their activation as it's the case for PLY produced by *Streptococcus pneumoniae* (Los *et al*., 2013; Paton *et al*., 1993).

1.4 – *Streptococcus pneumoniae* and its PFT, PLY

Streptococcus pneumoniae is a highly pathogenic Gram-positive bacterium, which predominantly infects the host *via* aerosol and colonizes the mucosal surfaces of the human upper respiratory tract, leading to asymptomatic carriage or severe invasive disease. *S. pneumoniae* is the major cause of lower respiratory infections and has been added, by the World Health Organization (WHO), as one of 12 priority pathogens in 2017, being ranked among the deadliest bacteria (https://www.who.int/news/item/27-02-2017-who-publishes-list-of-bacteria-for-which-new-antibiotics-are-urgently-needed). *S. pneumoniae* causes a wide range of infections including pneumonia, meningitis, sepsis, bacteremia and otitis media. Children younger than 5 years, due to their immature immune system, and the elderly, due to their inefficient immune system, are particularly susceptible to disease caused by *S. pneumoniae*. In addition to its infectious capacity, *S. pneumoniae* can remodel its genome contributing to its antibiotic resistance and evasion of vaccine-mediated immunity (Pereira *et al*., 2022; Weiser *et al*., 2018). Being a major health concern, *S. pneumoniae* and pneumonia that it causes, are currently considered an economic burden, resulting in over $17 billion annually in the United States (File Jr & Marrie, 2010), and at least €10.1 billion annually in Europe (Welte *et al*., 2012).

PLY is a 53-kDa β-PFT included in the CDC family. It is a major virulence factor of *S. pneumoniae* produced during infection by almost all clinical isolates and that can target virtually all host cell types (Gilbert *et al*., 1999; Tilley *et al*., 2005; Pereira *et al*., 2022). PLY was demonstrated essential to every stage of *S. pneumoniae* pathogenesis, having critical roles in the nasopharynx colonization, the progression of infection to neighboring tissues and the induction of inflammation (Figure 2) (Hirst *et al*., 2004; Pereira *et al*., 2022). Its importance in *S. pneumoniae* virulence has been demonstrated using *ply*-deficient mutant strains, which had been tested in mice and demonstrated to cause less-lethal infection and decreased injury, showing reduced overall virulence as compared to mice infected with wild-type PLY producer strains (Berry *et al*., 1992; Rubins & Janoff, 1998).

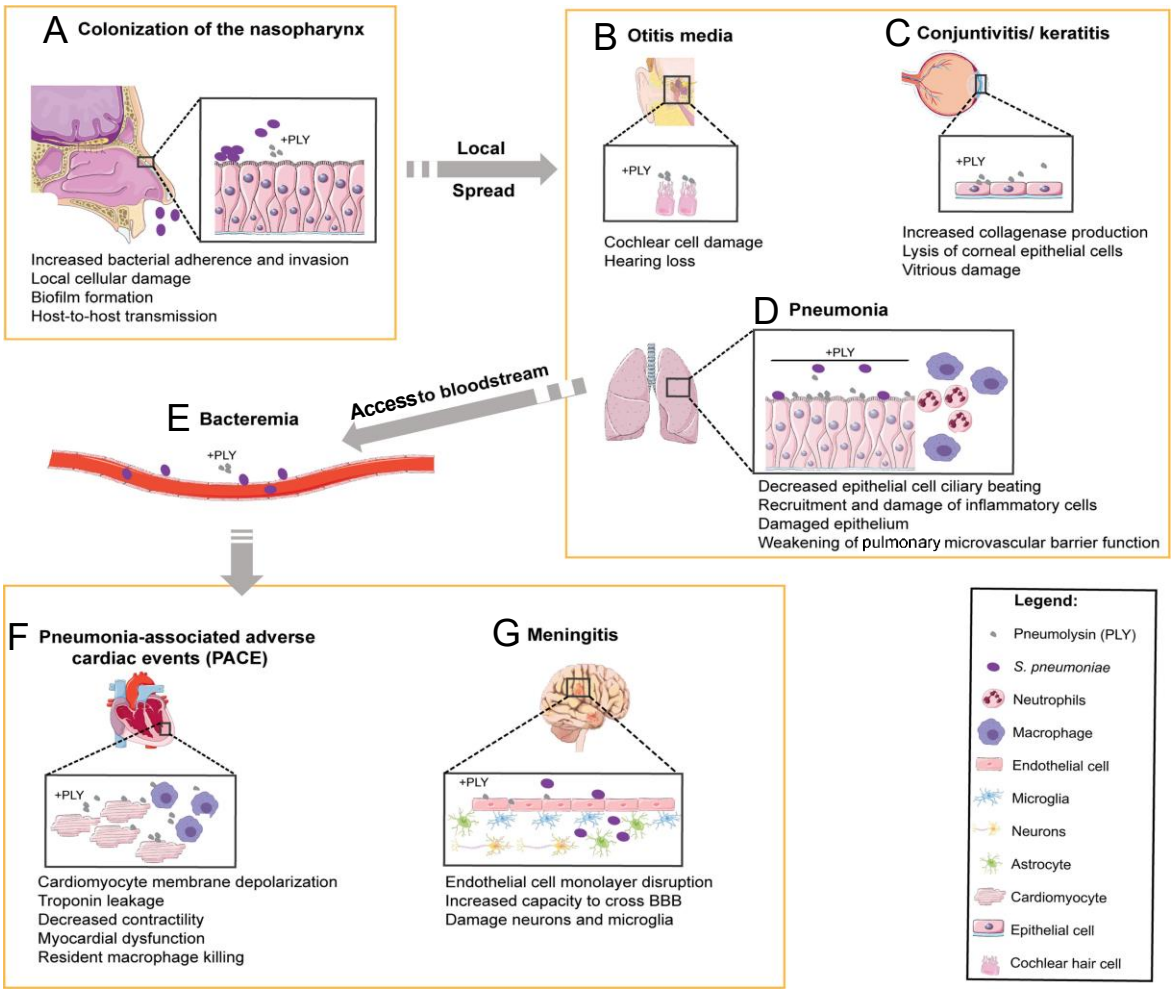

Figure 2: Role of PLY in human pathogenesis of *S. pneumoniae*. *S. pneumoniae* colonizes the human upper respiratory tract (A), and further colonization of the nasopharynx may lead to bacterial spread to neighboring tissues, namely, the middle ear (B) causing otitis media, the eyes (C) causing keratitis, and even the lower respiratory tract (D), causing pneumonia. From the lungs, *S. pneumoniae* can also reach the bloodstream (E) due to the PLY-induced dysfunction of epithelial barriers. The bacteria can also reach the heart (F), causing

pneumonia-associated adverse cardiac events, and even the brain (G), damaging both neurons and microglia. The effects associated to PLY are mentioned for every step of the infection. Reviewed and adapted from Pereira *et al*., 2022.

At the molecular level, PLY has the capacity to assemble into large transmembrane pores that disrupt PM integrity and cellular homeostasis (Pereira *et al*., 2022). As other PFTs, PLY is released as a water-soluble monomer, binds to cholesterol residues present in the PM of the host cells and oligomerizes forming a pre-pore complex. This pre-pore complex inserts into the membrane forming a transmembrane ring-shaped pore that allows an uncontrolled influx and efflux of ions and small molecules (Figure 3). The cellular responses and the extent of PLY-induced damage depends on PLY concentrations, which determine the number of pores, and on the influx of extracellular calcium. At high doses of PLY, the cells undergo irreversible damage and engage in programmed cell death (Figure 4). In turn, at sub-lytic PLY concentrations host cells respond by activating calcium-dependent repair pathways, which lead to cell survival (Pereira *et al*., 2022). In fact, the influx of extracellular calcium activates PM repair mechanisms, as well as protective cytoskeletal remodeling. However, an excess of calcium concentration is toxic for the cells, impairing host-cell signaling, damaging the cytoskeleton and causing cell death (Brito *et al*., 2019a; Wippel *et al*., 2011; Wolfmeier *et al*., 2015).

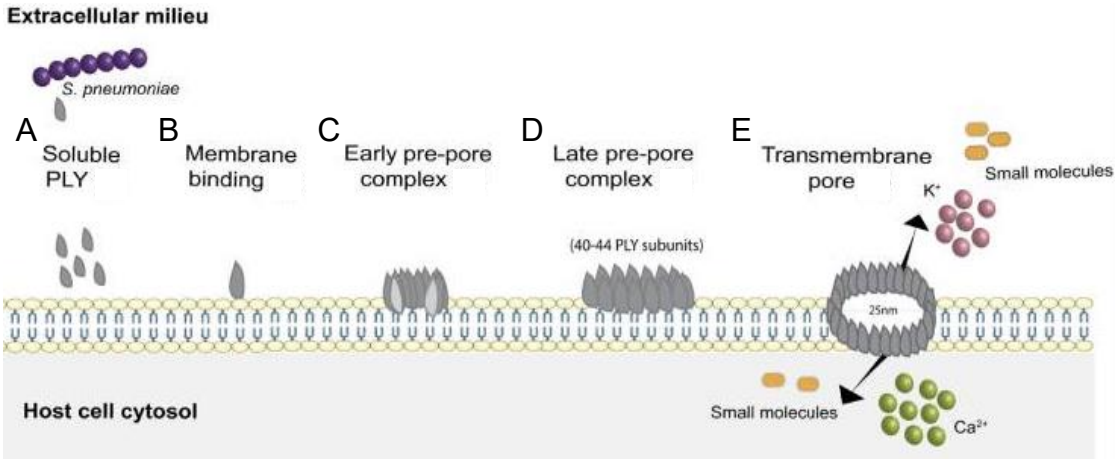

Figure 3: Schematic representation of the process of PLY pore formation, in the host PM. *S. pneumoniae* released PLY, as a water-soluble monomer (A), which binds cholesterol residues present on the surface of the host PM (B). By interacting between them, PLY monomers oligomerize and form an early pre-pore complex (C), which extends into the PM surface, completing its oligomerization and forming a late-pre-pore (D). Finally, PLY late-pre-pore complex inserts into the membrane, forming an open transmembrane channel (E), allowing an uncontrolled exchange of ions and small molecules between the intracellular and extracellular milieus. Reviewed and adapted from Pereira *et al*., 2022.

1.5 – Irreversible damage induced by PLY

At lytic doses, PLY causes overwhelming damage which leads to the massive entrance of calcium inside the cell. The uncontrolled elevation of intracellular calcium concentrations triggers a plethora of events that are deleterious for the cell, causing cell death and allowing the progression of the infection (Figure 4). In the lungs, PLY induces strong pro-inflammatory responses, which if exacerbated causes massive tissue damage that sustains the infection (Mitchell & Dalziel, 2014; Pereira *et al*., 2022).

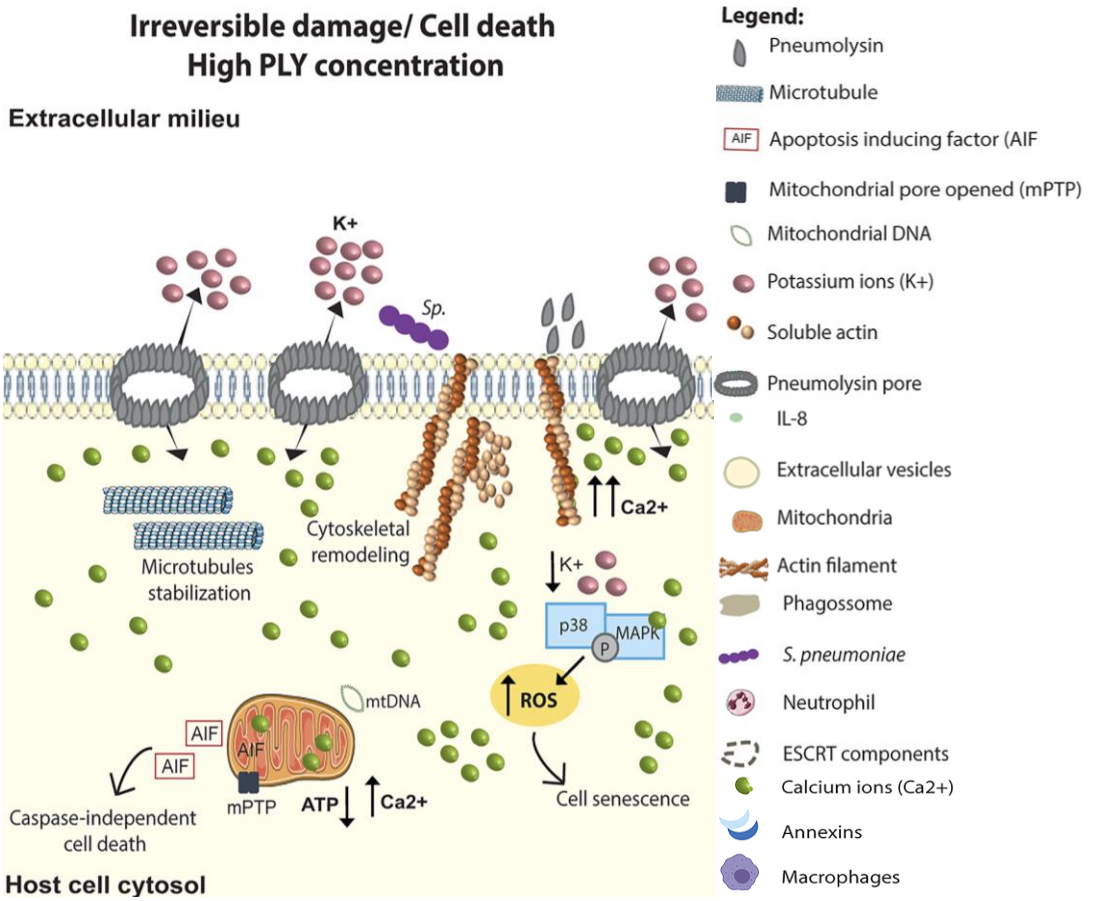

Figure 4: Overview of the irreversible damages leading to the progression of infection and cell death, due to high levels of PLY. The high influx of calcium into the cells facilitates *S. pneumoniae* adhesion due to the surface exposure of actin. PLY contributes to neuronal damage via microtubule stabilization which can perturb the axonal transport, and also by mitogen-activated protein kinases p38 (p38/MAPK) activation, which increases reactive oxygen species (ROS) production, inducing senescence. In addition, high levels of PLY also induce mitochondrial damage, leading to inflammation and programmed cell death. Reviewed and adapted from Pereira *et al*., 2022.

High amounts of PLY lead to irreversible mitochondrial damage, namely swelling, loss of membrane potential, and impairment in their metabolism. These alterations increase the mitochondrial permeability, reducing ATP levels, generating reactive oxygen species (ROS), and releasing mitochondrial DNA into the cytoplasm. Following its release to the cytosol, the mitochondrial DNA can be detected by innate immune receptors, contributing to inflammation (González-Juarbe *et al*., 2015; Nerlich *et al*., 2018). PLY induces necroptosis of alveolar macrophages and epithelial cells, which is mainly due to the necroptosis-initiating signals induced by mitochondrial damaged, such as the decrease of ATP and increased levels of ROS. Necroptosis depends on the activation and phosphorylation of mixed lineage kinase domain-like protein (MLKL), an effector of necroptosis, which is triggered by the calcium and potassium dysregulation in the cell (González-Juarbe *et al*., 2015; González-Juarbe *et al*., 2017). The rapid necroptosis-dependent depletion of alveolar macrophages contributes to extensive lung injury (Grommes & Soehnlein, 2011). In addition, high intracellular calcium induces actin exposure at the cell surface which contributes to *S. pneumoniae* adhesion and invasion.

Besides allowing an influx of calcium, PLY pores also allow the efflux of potassium, which triggers innate immune signaling and contributes to the pro-inflammatory responses. The decreased intracellular potassium concentrations trigger the activation of Nod-like receptor family pyrin domain-containing 3 (NLRP3) inflammasome, which consequently activates caspase-1 during *S. pneumoniae* infection. In the brain, caspase-1 activation induces pyroptosis of microglial cells, contributing to the pro-inflammatory cell death (Kim *et al*., 2015; Muñoz-Planillo *et al*., 2013).

1.6 – Cell repair mechanisms triggered by PLY

At sub-lytic concentrations, which presumably exist in the early stages of infection, PLY stimulates cell-autonomous repair mechanisms that overcome PM damage, restore cell integrity, and downregulate inflammation to promote cell survival (Anderson & Feldman, 2017; Pereira *et al*., 2022). The initial increase in intracellular calcium, due to the PLY pore formation, has thus a protective role against PLY intoxication (Bischofberger *et al*., 2012, Pereira *et al*., 2022). PM repair involves several events that are most probably interdependent in time and space (Brito *et al*., 2019a; Pereira *et al*., 2022). Indeed, cytoskeletal remodeling, pore clogging, PM blebbing and shedding of vesicles were already described as critical events for repair (Figure 5) (Brito *et al*., 2019a).

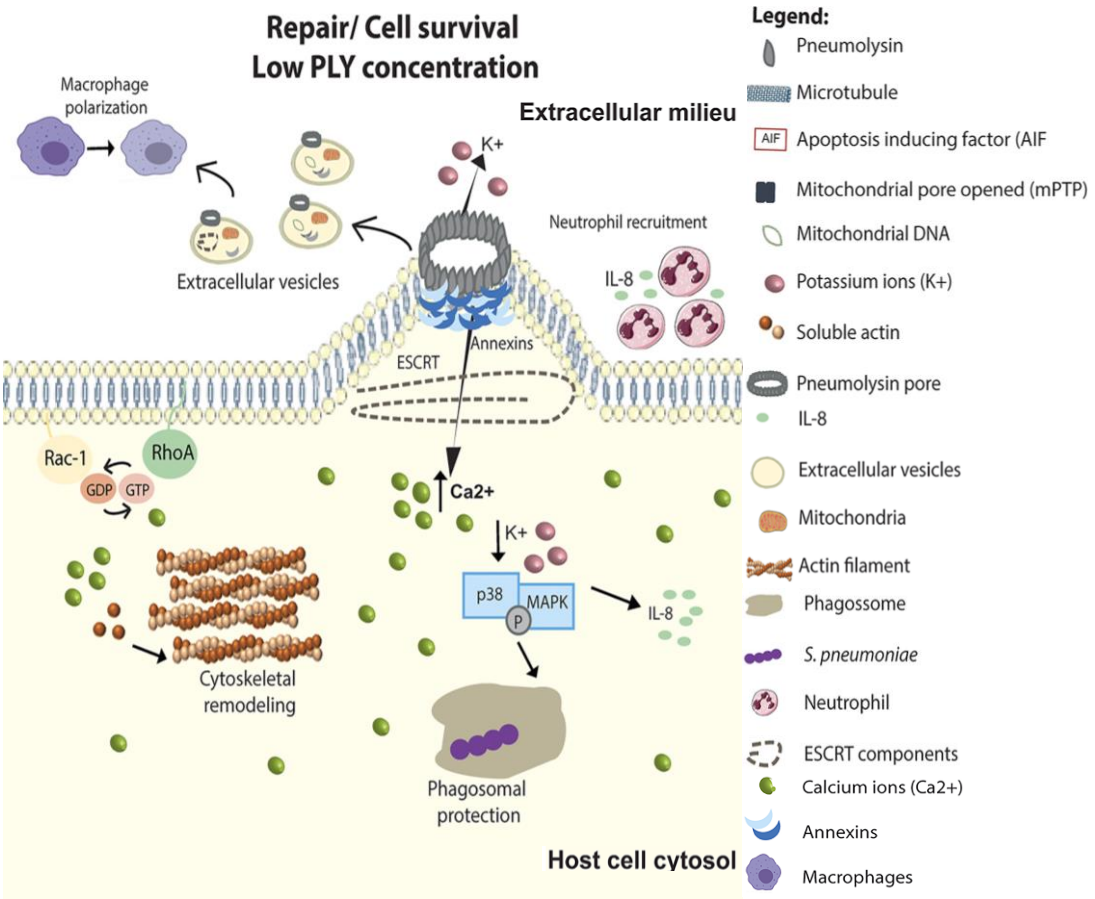

Figure 5: Schematic representation of the mechanisms of PM repair, allowing the recovery of PM integrity and cell survival upon intoxication with low levels of PLY. The initial and limited calcium influx triggers the recruitment of annexins that aggregate to clog the PM pore. The increase in calcium levels inside the cell also induces cytoskeleton remodeling triggering PM rearrangement, forming PM blebs and releasing vesicles containing PLY, in a process involving endosomal sorting complex required for transport (ESCRT) components. Also, the decrease in potassium levels, due to the pore formed by PLY, promotes p38/MAPPK activation, which prevents the cell from an excessive pro-inflammatory response. Reviewed and adapted from Pereira *et al*., 2022.

The influx of calcium induces actomyosin contraction that results in the disruption of the interactions between the cytoskeleton and the PM. This actomyosin remodeling decreases the membrane tension, which allows PM remodeling and leads to the formation of PM blebs and changes in the cell's shape (Babiychuk *et al*., 2011; Brito *et al*., 2019a). The formation of PM blebs is thought to isolate the damage and avoid excessive calcium entry. Calcium influx also leads to the recruitment of annexins, which are cytoplasmic proteins that translocate to the PM in a calcium-dependent manner, bind to PM phospholipids at the site of damage and aggregate at the basis of the blebs in 3D protein platforms that clog the pore. Annexins aggregation further isolate the damage and block the

continuous uncontrolled calcium entry until the damage is repaired (Jimenez & Perez, 2017; Mesquita *et al*., 2017; Potez *et al*., 2011; Wolfmeier *et al*., 2015).

It is well accepted that PM blebs formed in response to a PFT pore may either be released as extracellular vesicles or internalized and follow the degradation route, both mechanisms leading to pore elimination and damage repair. PLY at sub-lytic concentrations was shown to promote the release of extracellular vesicles which contains the pore (Babiychuk & Draeger, 2015; Wolfmeier *et al*., 2016; Alves, Pereira *et al*., in revision). PM blebbing and vesicle release of the damaged site involve endosomal sorting complex required for transport (ESCRT) proteins recruitment, which facilitates budding and vesicles release (Jimenez *et al*., 2014). Interestingly, extracellular vesicles released in the context of intoxication are enriched in annexins, PFT pores, ESCRT, and other molecules (Romero *et al*., 2017; Wolfmeier *et al*., 2016).

At low doses, PLY affects mitochondria in a more controlled manner than mentioned before. Indeed, PLY increases mitochondria permeability and contributes to the release of pro-apoptotic factors such as apoptosis-inducing factors (AIF), which once in the cytoplasm activate apoptosis without acute lysis, thus decreasing inflammation in tissues (Nerlich *et al*., 2018; Susin *et al*., 1999).

The efflux of potassium, induced by PLY and other PFTs, triggers mitogen-activated protein kinases p38 (p38/MAPK) pathways which are conserved responses involved in host defense responses (Cancino-Rodezno *et al*., 2009; Kloft *et al*., 2009; Porta *et al*., 2011). p38/MAPK is activated as a defense response against PFT-induced damage. p38/MAPK activation induces different stress responses in the cell, namely the unfolded protein response (UPR), a fundamental stress response from eukaryotic cells to protect the cell from the accumulation of unfolded protein during intoxication and to maintain cellular homeostasis. p38/MAPK, and subsequently UPR, activation is essential to prevent an excessive pro-inflammatory response that could result in tissue injury due to PLY intoxication (Aguilar *et al*., 2009; Bischof *et al*., 2008; Loose *et al*., 2015).

CHAPTER 2

Research context in the group of Cell Biology of Bacterial Infections

The group of Cell Biology of Bacterial Infections (CBBI) at i3S focus on the understanding of the mechanisms deployed by the host cell to survive and repair the PM in response to sub-lytic concentrations of different PFTs. The researchers concentrate their efforts in the identification of proteins and signaling pathways that are used by host cells to survive to low levels of intoxication, which presumably occurs at early stages of the infection. In an era where human bacterial pathogens are becoming resistant to antibiotics, increasing the risk for human health, the comprehension of cell membrane repair mechanisms may pave the way to new adjuvant approaches to fight bacterial infections.

2.1 – Hypothesis and preliminary data

Considering their previous data and the bibliography in the field, researchers from CBBI raise the hypothesis that shedding of extracellular vesicles is a major cellular mechanism to respond to PFT intoxication, to eliminate the toxin pore from the PM and thus to effective repair leading to the recovery of membrane integrity. To gain molecular understanding of these processes, CBBI researchers are addressing the specific role of the shedding of vesicles during intoxication. They seek for the identification of proteins and signaling pathways involved and for the understanding of how they cooperate to promote cell resistance against PFTs. Based on the assumption that proteins required for vesicle release and for PM repair might be enriched in the released vesicles, the vesicles released by cells intoxicated with PFTs (PLY and LLO) were collected, isolated and their proteomic content was identified by Mass Spectrometry analysis (Figure 6). The abundance of the identified proteins in vesicles released by intoxicated cells was compared to their abundance in control vesicles released by non-intoxicated cells cultured under standard or serum-starvation conditions (Figure 6.A). In addition, the abundance of the proteins in the vesicles was also compared with their corresponding abundance in the cells that released the vesicles (Figure 6.B).

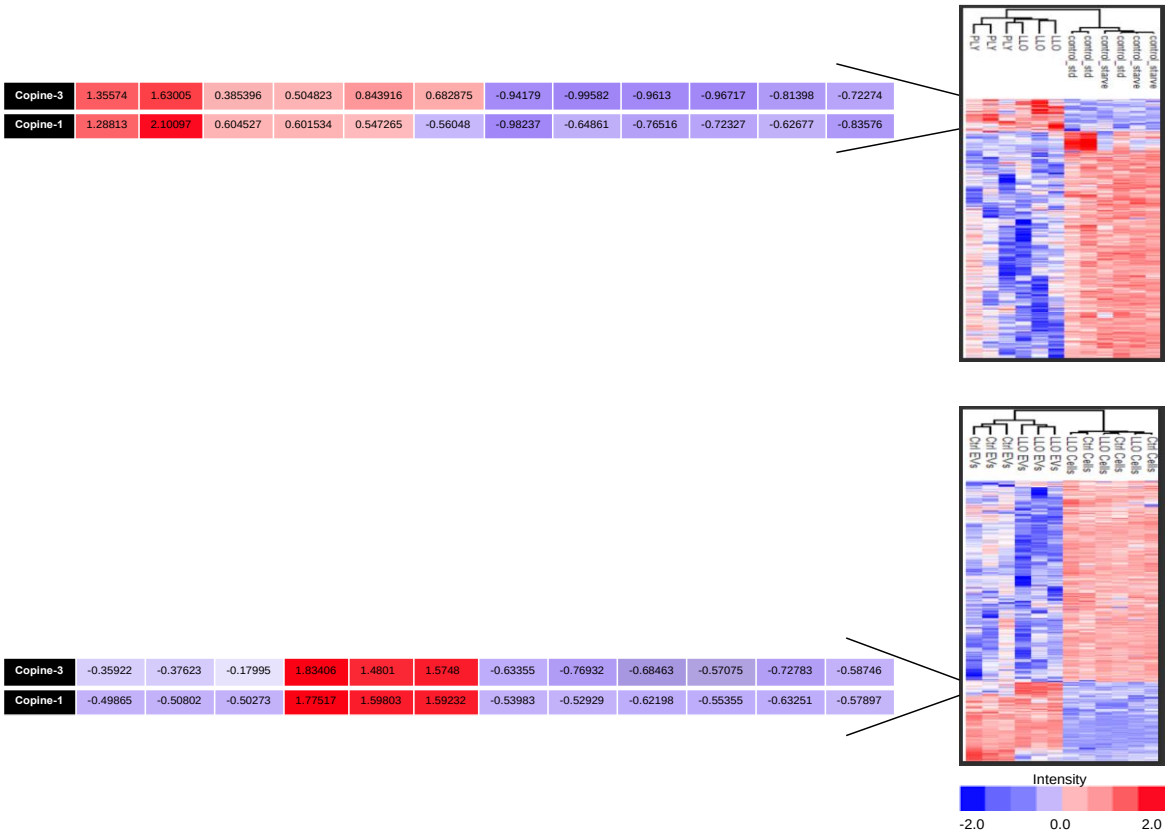

Figure 6: Heat maps of the proteins showing significantly different abundances in vesicles from intoxicated cells as compared to non-intoxicated ones. The intensity of proteins is represented by fold change. In red are indicated the proteins overrepresented in a specific condition. In blue are shown the proteins underrepresented. A: Data obtained by comparing the proteomic profile of vesicles from intoxicated cells to vesicles released from control non-intoxicated cells. The overrepresentation of copine-1 and copine-3 in vesicles released by cells intoxicated by PLY or LLO is highlighted; B: Data obtained by comparing the proteomic content vesicles released by LLO-intoxicated cells as compared to the total cellular content of these cells. The overrepresentation of copine-1 and copine-3 in the vesicles released from intoxicated cells as compared to control vesicles and to the cells is highlighted.

Copine-1 (CPNE1) and copine-3 (CPNE3) were abundantly detected in the vesicles released by intoxicated cells and almost undetectable in vesicles released by control cells (Figure 6.A). In addition, they were found enriched in vesicles released by LLO-intoxicated cells as compared to the full proteomic content of the cells (Figure 6.B). These findings suggest that copine-1 and copine-3 are selectively sorted into the vesicles released upon intoxication, which may indicate that they have an important role in vesicle formation and damage repair.

2.2 – Copine-1 and copine-3

Copines are a family of highly conserved phospholipid membrane-binding proteins including nine soluble cytoplasmic proteins in humans. They are found in different

eukaryotic organisms, ranging from plants to animals, and were first discovered in *Paramecium tetraurelia*. Copines are expressed in a variety of mammalian tissues, including the brain, heart, kidney, liver, lung and spleen (Creutz *et al*., 1998; Tomsig & Creutz, 2000; Tomsig & Creutz, 2002; Tomsig *et al*., 2003). They are calcium-sensitive proteins able to translocate to the PM, and/or to the nucleus (copine-1, -2, -3 and -7) in response to increased levels of intracellular calcium (Perestenko *et al*., 2010). It was also shown that copines promote lipid vesicle aggregation in a calcium-dependent manner (Creutz *et al*., 1998).

The different copines share a common structure with two N-terminal C2-domains, C2A and C2B, followed by a C-terminal von Willebrand factor A-domain (vWA) (Figure 7). The sequence of the A-domain found in copines is structurally related to the vWA domain found in integrins. These domains exist in several membrane-bound proteins and are involved in cellular signaling pathways. Indeed, the majority of A-domains are present in extracellular matrix proteins, like integrins, and are important in the mediation of protein-protein interactions. Nevertheless, a sequence database search for A-domains showed that A-domains can also be found in intracellular proteins (Damer *et al*., 2005, Whittaker & Hynes, 2002). Among those proteins, copines were the first intracellular proteins for which an A-domain has been described (Creutz *et al*., 1998). Copines can interact with different target proteins via the A-domain, such as mitogen-activated protein kinase/extracellular signal-regulated kinase kinase (MEK1) and protein phosphatase 5 (PP5), both involved in MAPK signaling (McCain, 2013; Tomsig *et al*., 2003; Tomsig *et al*., 2004; Zhou *et al*., 2004). In addition to the A-domain, copines possess a variable-length C-terminal domain, which may confer unique characteristics to the different copines (Creutz *et al*., 1998; Tang *et al*., 2021; Whittaker & Hynes, 2002).

The C2 domains are known as calcium-dependent phospholipid-binding motifs, as they contain calcium-binding sites. Proteins containing C2 domains were described to be involved in membrane trafficking, and regulate vesicle transport. In response to a rise in intracellular calcium, the C2 domains bind to calcium via specific aspartate amino acid residues (Corbalan-Garcia & Gómez-Fernández, 2014; Damer *et al*., 2005; Ilacqua *et al*., 2018; Nalefski & Falke, 1996). Upon calcium binding, the C2B domain, with the support of the C2A domain, induces translocation by promoting the binding of copines to the phospholipid bilayer of the PM (Perestenko *et al*., 2015).

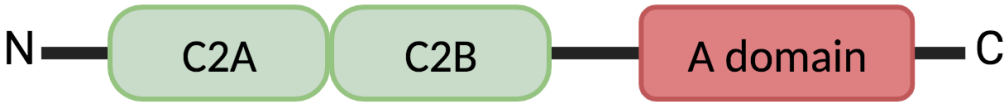

Figure 7: Schematic representation of the structural domains of copines. The C2 domains contains the calcium binding sites. The A-domain is known as a protein-protein interaction domain. Created with BioRender.com

Different members of the copine family are simultaneously expressed in the same cell, as it was first demonstrated for copine-1 and copine-3 in the cytosol of human neutrophils. Copine-1 and copine-3 are ubiquitously expressed and share the highest sequence homology among the copine family (Caudell *et al*., 2000; Cowland *et al*., 2003; Tomsig & Creutz, 2002). Despite their functions remain unknown, it has been hypothesized that copines are important in signaling processes on membrane surfaces due to their capacity to bind with PM and target proteins, through an increase of intracellular calcium (Tomsig *et al*., 2003).

2.3 – My project

Considering the characteristics of CPNE1 and CPNE3, particularly their calcium responsiveness and their ability to translocate to the PM, and the fact that they were found in higher abundance in vesicles released by intoxicated cells than by control cells, we hypothesized that they could have an important role in the repair of damage through the secretion of extracellular vesicles. To test this hypothesis, we will follow two different approaches using key molecular tools already available in the lab. In the first approach, we aim to evaluate the ability of cells depleted for the expression of CPNE1 or CPNE3 to repair from damage caused by PLY and recover PM integrity. For that, we will use cell lines knockout for the expression of copine-1 or copine-3 obtained by CRISPR/Cas9 in the CBBI. With the second approach, we aim to assess by confocal microscopy the intracellular localization of copine-1 and copine-3 in control and intoxicated cells, using plasmids allowing the expression of copine-1 and copine-3 in fusion with GFP, also available in the laboratory.

CHAPTER 3

Material and Methods

3.1 – Cell lines

HeLa cells (ATCC CCL-2) were grown in complete Dulbecco's Modified Eagle Medium with high glucose, L-glutamine and sodium pyruvate (DMEM; Biowest), supplemented with 10 % Fetal Bovine Serum (FBS; Biowest), and maintained in a 5 % CO_2 atmosphere at 37 ºC.

3.2 – Transfection of HeLa cells

Different plasmids (Table 2) expressing GFP already available in the laboratory, were purified from *Escherichia coli* stocks cultured in Luria-Bertani (LB) medium with 30 µg/mL kanamycin, using the NZYSpeedy Miniprep kit (NZYTech) according to the manufacturer's instructions and quantified with a NanoDrop One spectrophotometer.

Table 2: Plasmids used for transfection of HeLa cells.

pEGFP-C1 (GFP-C1)	Control
pEGFP-*CPNE3* (GFP-CPNE3)	Fusion between pEGFP-C1 and *CPNE3* fragments
p*CPNE3*-EGFP (CPNE3-GFP)	Fusion between pEGFP-N2 and *CPNE3* fragments
pEGFP-*CPNE1* (GFP-CPNE1)	Fusion between pEGFP-C1 and *CPNE1* fragments

HeLa cells ($3.0x10^5$) were plated in a 6-well plate containing glass coverslips to allow further immunofluorescence analysis. For flow cytometry analysis or immunoblot, cells were directly grown on plastic wells. The day after, the cells were transfected using JetPRIME (Polyplus) following the manufacturer's protocol: 3 µg of each plasmid was mixed with 200 µL of JetPRIME buffer and 9 µL of JetPRIME reagent and the mix was added to the cells. After 4 h, the wells were washed twice in Dulbecco's Phosphate Buffered Saline 1x (DPBS; Lonza), fresh complete medium was added and cells were incubated at 37 ºC for 24 h.

HeLa cells were washed twice in DPBS 1x and were processed for different experiments: flow cytometry analysis, microscopy, and immunoblotting. Non-transfected cells were used as control.

3.3 – Flow Cytometry analysis

Transfected cells were trypsinized (Tryple/Express, Invitrogen), resuspended in 350 μL of FACS buffer (2 % FBS in DPBS 1x), and filtered to eppendorf tubes before flow cytometry analysis. Cells were analyzed in a BD Accuri C6 Plus flow cytometer (BD Biosciences), the populations of interest were selected following different parameters: size/complexity to select living cells, size/height to select single cells and the fluorescence detector channel FL1-A to detect the cells that express GFP. In each experiment, at least 15 000 cells were analyzed and data were analyzed using FlowJo (TreeStar).

Intoxicated cells (see 3.9) and non-intoxicated controls were washed twice in DPBS 1x, trypsinized, resuspended in FACS buffer and filtrated before flow cytometry analysis in a BD Accuri C6 Plus flow cytometer. Just before the analysis 2 μg/mL Propidium Iodide (PI, Sigma, 81845) was added to the cell suspensions and incubated for 1 min at room temperature, to discriminate permeable from non-permeable cells. Different gates were established to select the populations of interest, namely living cells (size/complexity), single cells (size/height) and PI-positive cells, obtained using the FL3-A fluorescence detector channel. In each experiment, at least 16 000 cells were analyzed, and data were analyzed using FlowJo.

3.4 – Immunofluorescence microscopy analysis

Cells seeded in coverslips were fixed in 300 μL of 4 % paraformaldehyde (PFA, Electron Microscopy Sciences) for 15 min at room temperature and washed in DPBS 1x. Cells on coverslips were then processed for fluorescence labelling. Coverslips were placed in a wet chamber and cells permeabilized with 0.2 % Triton X-100 (Sigma-Aldrich, T8532) in DPBS 1x for 5 min and washed in DPBS 1x. To evaluate the efficacy of transfection and the expression of the GFP-tagged proteins, nuclei were also stained using DAPI (Sigma-Aldrich, D9542) diluted at 1:1000 in DPBS 1x for 30 min at room temperature, in the dark. The coverslips were then mounted onto microscope slides using Aqua-Poly/Mount (Polysciences) and cells were visualized under a fluorescence Olympus BX63 microscope using a 40 x 0.85 objective and the images were processed using ImageJ. To assess the intracellular localization of CPNE1 and CPNE3 in intoxicated cells, the cells were incubated with rabbit anti-myosin IIA antibody (Anti-NMHCIIA, Sigma-Aldrich, M8064), diluted at 1:500

in 0.1 % Bovine Serum Albumin (Sigma-Aldrich, A7906; BSA) in DPBS 1x for 1 h at room temperature. Coverslips were washed twice in DPBS 1x and incubated for 45 min at room temperature with anti-rabbit antibody conjugated with Cy3 (Jackson ImmunoResearch, AB_2338006), diluted at 1:200 in BSA 0.1% and DAPI diluted at 1:1000 in BSA 0.1%. Finally, coverslips were washed twice in DPBS 1x and once in H_2O and mounted onto microscope slides. The cells were visualized with a Leica Scanning Confocal SP5 equipped with a 63 x 1.30 Glycerol objective lens. The images were processed using ImageJ.

3.5 – Western Blot analysis

Transfected and non-transfected cells were lysed with 50 μL/well of Laemmli buffer (0.25 mM Tris–HCl, pH 6.8; 10 % SDS; 50 % glycerol; and 5 % β-mercaptoethanol) and denatured at 94 ºC for 10 min.

The samples were loaded into a 10 % acrylamide gel and run at 140 V to separate proteins according to their molecular weight. The separated proteins in the acrylamide gel were then transferred to a nitrocellulose membrane in a Trans-Blot Turbo Transfer System (Bio-Rad) at 0.3 A and 25 V for 1 h. After the transfer, the nitrocellulose membrane was stained with Ponceau S Staining solution (Sigma-Aldrich, P7170), incubated in 5 % low-fat milk in TBS-T 1x (blocking solution: 150 mM NaCl; 50 mM Tris–HCl, pH 7.4 with 0.1 % of Tween 20 (Sigma-Aldrich, P1379)) under agitation in roller mixer for 1 h at room temperature.

For the immunoblotting detection of GFP, the membrane was incubated overnight at 4 ºC with an anti-GFP antibody (Santa Cruz Biotechnology, sc-9996) diluted at 1:500 in 2.5 % low-fat milk in TBS-T 1x, under agitation. For detection of CPNE1, the nitrocellulose membrane was incubated overnight at 4 ºC with an anti-CPNE1 antibody (Santa Cruz Biotechnology, sc-101269) diluted at 1:250 in 2.5 % low-fat milk in TBS-T 1x, under agitation. Finally, for detection of CPNE3, the membrane was incubated overnight at 4 ºC with an anti-CPNE3 antibody (Santa Cruz Biotechnology, sc-390143) diluted at 1:500 in 2.5 % low-fat milk in TBS-T 1x, under agitation. The membrane was washed 3 times for 15 min with TBS-T 1x, at room temperature and incubated with the secondary antibody anti-mouse conjugated with Horseradish Peroxidase (HRP) (Abliance, BI 2413C) diluted at 1:1000 and agitated in the roller mixer for 1 h, at room temperature. The membrane was again washed 3 times with TBS-T 1x and the signal was detected using Pierce Enhanced Chemiluminescence (ECL) Western Blotting substrate (Thermo Fisher Scientific, 32106) following the manufacturer's instructions. Briefly, the membrane was incubated with the

substrate for 1 min at room temperature and protein bands were detected by a Molecular Imager ChemiDoc XRS+ System (Bio-Rad) coupled with Image Lab Software. Actin detection was used as a loading control by using an anti-actin monoclonal antibody (Sigma-Aldrich, AC 15, A5441) diluted at 1:5000 in 2.5 % low-fat milk in TBS-T 1x, under agitation 1 h, at room temperature. The membrane was then washed 3 times with TBS-T 1x and incubated with anti-mouse-HRP diluted at 1:1000 in 2.5 % low-fat milk in TBS-T 1x under agitation and agitated in the roller mixer for 1 h at room temperature.

3.6 – Isolation of genomic DNA from HeLa cells

Genomic DNA (gDNA) was extracted from HeLa cells wild-type (WT), knockout for copine-1 (KO *CPNE1*) and knockout for copine-3 (KO *CPNE3*) using Maxwell Rapid Sample Concentrator (RSC, Promega) following the protocol provided with the Whole Blood DNA kit (Promega). Briefly, the three variants of HeLa cells were grown to confluence in T75 cell culture flasks, washed twice in DPBS 1x, trypsinized and counted, using a Neubauer chamber. The volume corresponding to $5x10^6$ cells was centrifuged at 1200 rpm for 5 min. The Lysis Buffer containing Proteinase and RNase A was added to the pelleted cells and incubated for 10 min at room temperature. Lysates were centrifuged at 8000 xg for 2 min to eliminate the cell debris. Maxwell RSC cartridges were prepared, one for each cell line, placing plungers in well #8 and elution tubes containing elution buffer at the end of each cartridge. The samples were run on the Maxwell RSC instrument (Promega) using the Whole Blood DNA protocol, according to the manufacturer's instructions. gDNA concentration was determined using a NanoDrop One spectrophotometer (Thermo Fisher Scientific), which also allows the evaluation of contaminations with proteins (A_{260}/A_{280}) and reagents (A_{230}/A_{280}).

3.7 – PCR amplification of the regions flanking the cut sites

The genomic DNA extracted from KO *CPNE1* and KO *CPNE3* cells was used as template together with the primers flanking the region where the cut was expected to occur in the *CPNE1* or *CPNE3* gene (Table 3). gDNA from WT HeLa cells was used as control with those same primers.

Table 3: Sequence of the primers targeting the regions that flank the expected cut site in *CPNE1* and *CPNE3* sequences.

CPNE1 Exon 4 Forward	5' GGA CAT CGG CTC CAA GTC TG 3'
CPNE1 Exon 10 Reverse	5' GAG GAG GTG AGG AAG GCA GC 3'
CPNE3 Exon 4 Forward	5' GGT GTA GGT TGA GCG CAC AG 3'
CPNE3 Exon 13 Reverse	5' CCT AAC CAC CAA CCT GGT GC 3'

PCR was performed using KAPA2G Fast ReadyMix PCR kit (KAPABiosystems) according to the manufacturer's protocol and the following cycling conditions: 3 min at 95 ºC for initial denaturation, 15 s at 98 ºC for denaturation, 15 s at 55 ºC for primer annealing and 1 min at 72 ºC for extension. Denaturation, annealing and extension were repeated for 30 cycles. PCR products were run in an 0.8 % agarose electrophoresis gel with GreenSafe (NZYTech). Following electrophoresis, the amplified fragments were detected in a Molecular Imager Gel Doc XR+ System (Bio-Rad) coupled to Image Lab Software (Bio-Rad).

3.8 – Sanger sequencing

The PCR products showing the expected molecular weight on the agarose gel were sliced and the corresponding DNA extracted using the Gel Pure NZY Tech kit (NZYTech) according to the manufacturer's instructions. The concentrations of the obtained purified DNA were determined using a NanoDrop One spectrophotometer and 50 ng of each DNA fragment was sent for sequencing (Eurofins Genomics) with the primers listed in Table 3.

3.9 – Intoxication with PLY

HeLa WT, KO *CPNE1* and KO *CPNE3* cells ($3x10^5$) were seeded in 6-well plates and maintained at 37 ºC. The day after, the cells were washed twice using Hank's Balanced Salt Solution with calcium and magnesium (HBSS, Lonza) and intoxicated with growing or the indicated concentrations of PLY (0.05; 0.10; 0.17 and 0.25 nM) previously diluted in HBSS, for 10 min at 37 ºC. After intoxication, cells were washed twice in DPBS 1x and were processed for different analyses. For flow cytometry analysis (see 3.3) they were trypsinized, resuspended in FACS buffer and filtrated. For immunofluorescence, they were fixed in glass coverslips for 15 min in PFA 4 % at room temperature, washed with DPBS 1x and quenched with 0.1 M ammonium chloride (NH_4Cl) at 4 ºC for 30 min. Then, cells were washed again in DPBS 1x and processed for immunofluorescence labelling (see 3.4).

For the recovery of the plasma membrane permeability by flow cytometry analysis, HeLa WT, KO *CPNE1* and KO *CPNE3* cells ($3.0x10^5$) were seeded in 6-well plates. The

day after, cells were washed twice with HBSS, intoxicated with PLY at 0.17nM for 10 min at 37 ºC, and then washed again twice with DPBS 1x. Cells were allowed to recover in complete medium for different time points ranging from 0 to 120 min, and processed for flow cytometry analysis (see 3.3).

3.10 – Automated high-throughput Imaging of PLY-treated cells

HeLa WT and KO *CPNE1* cells ($2x10^5$) were seeded in 96-well microplates (PhenoPlate, PerkinElmer) and allowed to grow for 18 h at 37 ºC. Cells were washed once with HBSS and incubated with 50 μL/well of Hoechst at 10μg/mL (Invitrogen, H3570) diluted in HBSS, at room temperature for 15 min in the dark to stain the nuclei. Next, 50 μL of HBSS containing PI at 25 μg/mL and PLY (at growing concentrations 0.10; 0.25; 0.50 and 1nM) was added. Non-intoxicated condition (without PLY) was used as control for basal permeabilization level. The plate was placed in an IN Cell Analyzer 2000 (GE Healthcare), which maintains the cells at 37 ºC with 5 % of CO_2. The permeabilization of cells was followed in real-time for 15 min and visualized in the Cy3 channel (detecting the PI fluorescence). To control the number of cells throughout the experiment each well was also followed in the DAPI channel (detecting the Hoechst signal). The analysis was done for each PLY concentration at the time in 3 technical replicas. Two pictures from two different fields were taken per minute in each well. The images recorded by the IN Cell Analyzer 2000 were analyzed using the IN Cell Developer Toolbox (GE Healthcare) software, which allows to count the total number of cells by counting the nucleus stained by Hoechst, and identify the PI-positive cells applying a manual fluorescence intensity threshold.

3.11 – Statistical analysis

Statistical analyses were carried out with Prism GraphPad software version 8.3.0 (GraphPad Software, San Diego, California USA, www.graphpad.com). Two-way ANOVA followed by Dunnett's Multiple Comparison was used to compare the mean of samples against a control group mean, within each condition.

CHAPTER 4

Results and Discussion

4.1 – Validation of the expression of the GFP-tagged CPNE1 and CPNE3

To determine the intracellular localization of copine-1 (CPNE1) and copine-3 (CPNE3) in response to intoxication and gain insights on their putative role during repair responses induced by sub-lytic doses of PLY, plasmids allowing the expression of CPNE1 and CPNE3 in fusion with GFP were previously obtained in the laboratory. We started by validating the expression of the GFP-tagged versions of CPNE1 and CPNE3. To do so, HeLa cells were transfected with the different plasmids (Table 2) and the expression of the fusion proteins was analyzed by different methods: flow cytometry, fluorescence microscopy and western blot.

Cells were transfected with pEGFP-C1 as control, pEGFP-*CPNE3*, p*CPNE3*-EGFP and pEGFP-*CPNE1* and GFP expression was evaluated by flow cytometry. Under the flow cytometer, we first defined the population of live cells and exclude the debris, by evaluating the area (FSC-A) and complexity (SSC-A) of the events. Living cells are bigger and more complex than debris, so the population closer to 0 was defined as debris and was excluded (Figure 8.A). We also defined a population of single cells, in which duplets were excluded from the population of live cells, by evaluating area (FSC-A) and height (FSC-H) (Figure 8.B).

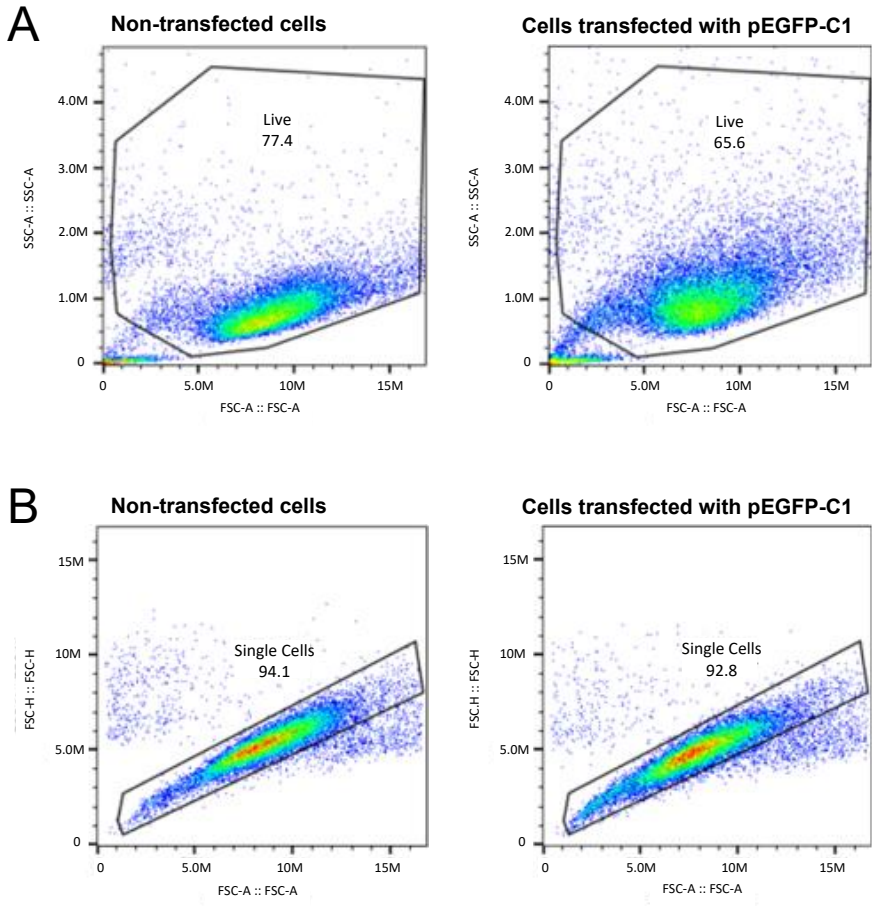

Figure 8: Representative flow cytometry plots obtained from non-transfected cells and cells transfected with the control plasmid pEGFP-C1. A: Shows the population of live cells defined by area and complexity; B: Shows the population of single cells defined by area and height.

The non-transfected cells were used to establish a threshold of autofluorescence defining a population of cells that do not express GFP (GFP-negative cells). This threshold was applied to the samples of transfected cells to determine the population of cells expressing GFP. Representative histograms of non-transfected and pEGFP-C1 transfected cells are shown below (Figure 9). According to the defined threshold, while non-transfected sample only contained 1.5 % of cells considered GFP positive, in the transfected sample 75 % of the cell population was positive for GFP expression (Figure 9).

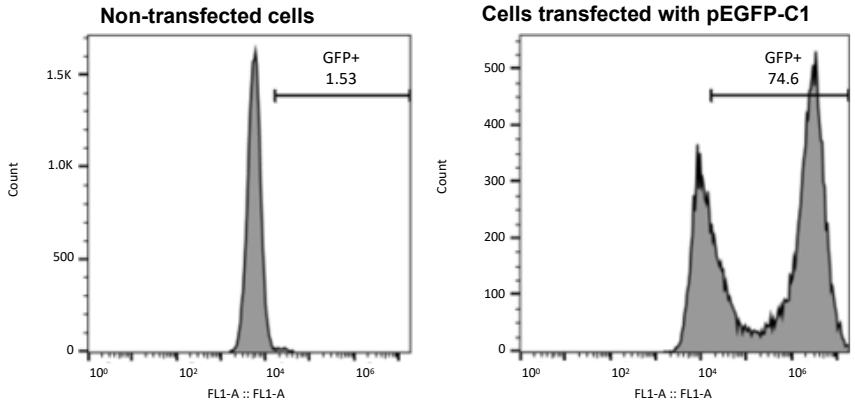

Figure 9: Single parameter histograms representative of non-transfected cells (left panel) and cells transfected with the control plasmid pEGFP-C1 (right panel). The y-axis shows the number of events counted and the intensity of the measured fluorescence is indicated in the x-axis. The threshold defined by the autofluorescence of the non-transfected cells is indicated. The percentage of cells that express GFP in non-transfected and transfected cells is also indicated.

The percentage of GFP-positive cells was determined for each sample of transfected cells by applying the same threshold defined above. While, as expected, the percentage of GFP expressing cells was residual in non-transfected samples, at least 60 % of the transfected cells expressed GFP (Figure 10). This indicates that each of the plasmids used to transfect the cells allowed the expression of GFP, whether the transfected cells correctly express the GFP-tagged CPNE1 or CPNE3 cannot be addressed by flow cytometry.

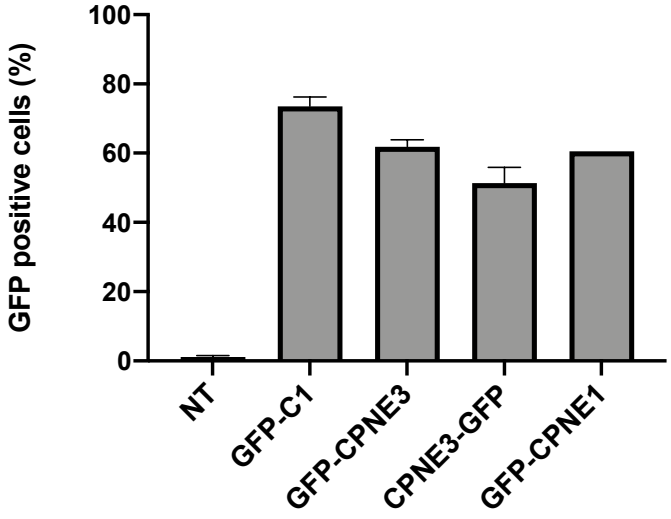

Figure 10: Graph showing the percentage of GFP-positive cells, determined by flow cytometry, in non-transfected cells (NT) and samples of cells transfected with pEGFP-C1, pEGFP-*CPNE3*, p*CPNE3*-EGFP or pEGFP-*CPNE1*. Results are the mean ± SEM of 2 experiments.

We next evaluated the expression of the GFP-tagged CPNE1 and CPNE3 by fluorescence microscopy. As for flow cytometry analysis, HeLa cells were transfected with the plasmids listed in Table 2 which allow the expression of GFP alone (pEGFP-C1) or the expression of CPNE1 or CPNE3 fused to GFP. Cells were stained with DAPI, which binds DNA and labels the nuclei and the GFP fluorescence was detected in the FITC channel (Figure 11).

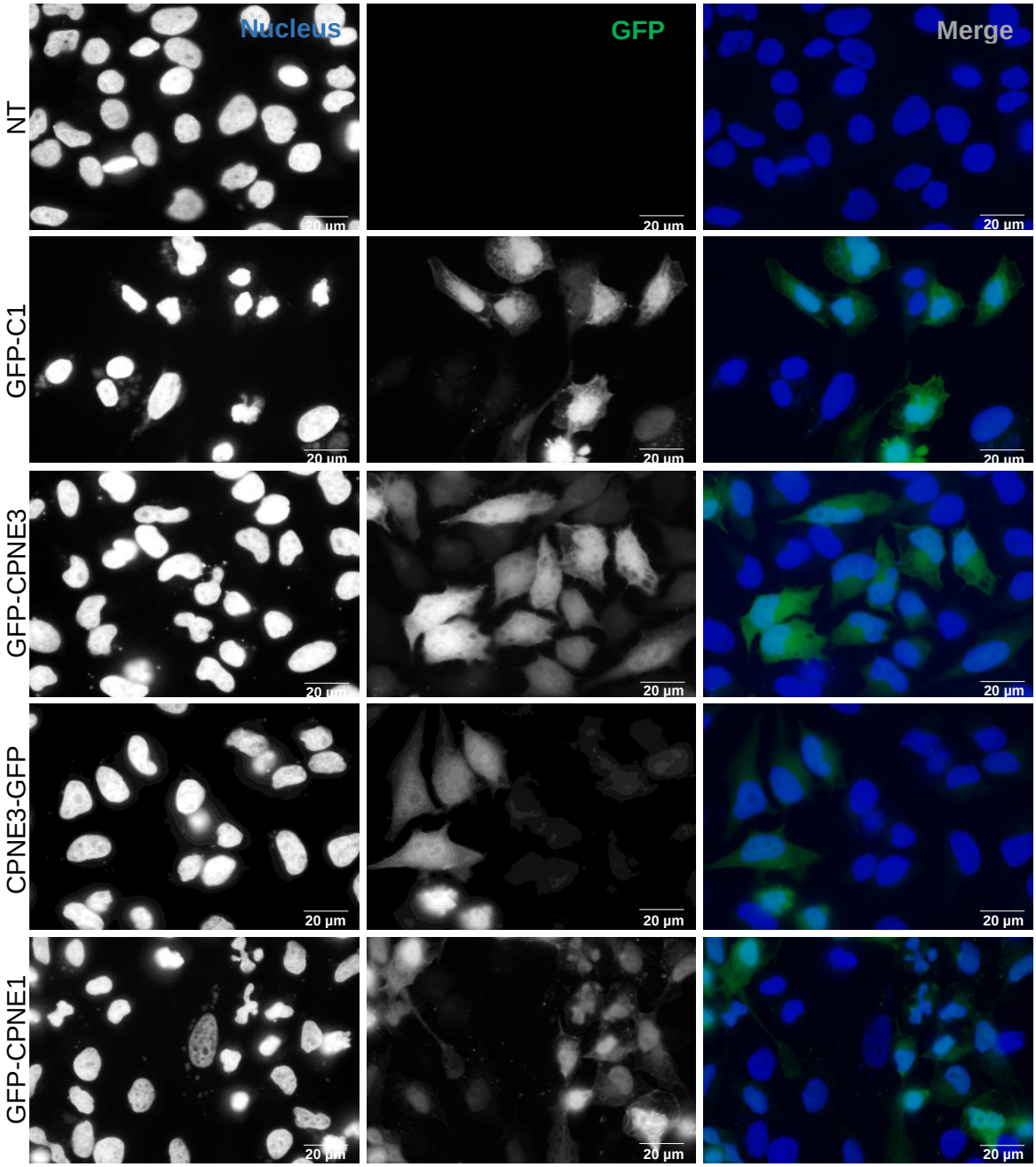

Figure 11: Fluorescence microscopy images of non-transfected cells (NT), cells transfected with pEGFP-C1, pEGFP-*CPNE3*, p*CPNE3*-EGFP or pEGFP-*CPNE1*. The nuclei are detected by DAPI staining (blue). GFP is shown in green. Scale bar: 20 µm.

In agreement with the results obtained by flow cytometry analysis (Figure 10), GFP is detected in all the samples of transfected cells, while non-transfected cells do not show GFP associated fluorescence. The GFP signal is uniformly distributed in the cytoplasm of transfected cells, indicating that the GFP-tagged proteins do not have a particular localization within the cell. Cells transfected with the plasmid p*CPNE3*-EGFP display weaker GFP signals than cells transfected with the other plasmids, which suggests that the expression of CPNE3-GFP is lower than the other GFP variants (Figure 11).

Finally, the expression of the fusion proteins was validated by Western Blot using an anti-GFP antibody. Total protein extracts from transfected and non-transfected cells were separated by SDS-PAGE electrophoresis and proteins were transferred to a nitrocellulose membrane. The membrane was incubated with an anti-GFP antibody. Since CPNE1 has a molecular weight of 59 kDa, CPNE3 has a molecular weight of 60 kDa, and the GFP alone accounts for 27 kDa, we expected to detect a band of about 90 kDa in the cells transfected with pEGFP-*CPNE1*, pEGFP-*CPNE3* and p*CPNE3*-EGFP and a band of 27 kDa for the cells transfected with the pEGFP-C1 control plasmid CPNE1 (Figure 12). As a loading control, we detected actin (42 kDa) using an anti-actin antibody.

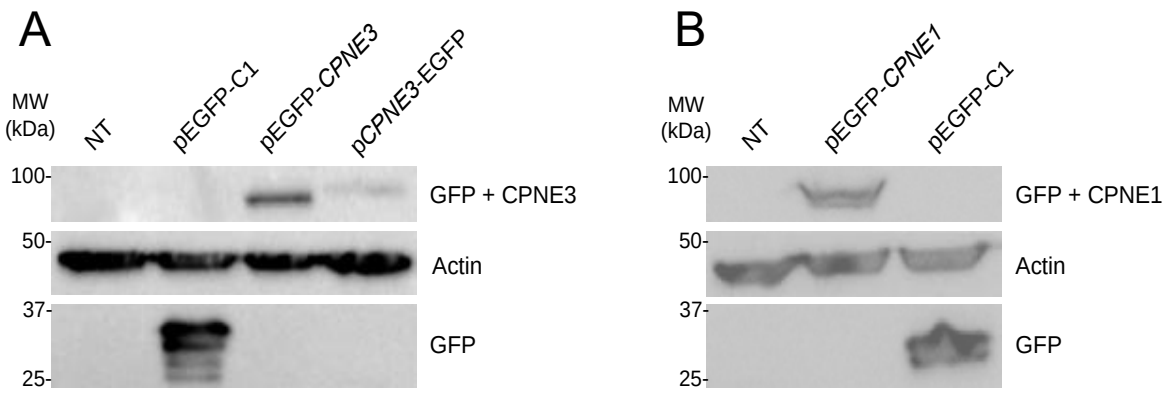

Figure 12: Immunoblot on total extracts of non-transfected (NT) or transfected cells, revealed using an anti-GFP antibody. A: Immunoblot for the detection of the fusion between GFP and CPNE3 in non-transfected cells (NT), cells transfected with control pEGFP-C1, pEGFP-*CPNE3* and p*CPNE3*-EGFP; B: Immunoblot for the detection of the fusion between GFP and CPNE1 in non-transfected cells (NT), cells transfected with pEGFP-C1 and pEGFP-*CPNE1*. Actin was detected as loading control. Molecular weights (MW) of the reference protein ladder are indicated.

As expected, in the lanes corresponding to the cells transfected to express the GFP-tagged CPNE1 and CPNE3 proteins (GFP-CPNE3, CPNE3-GFP and GFP-CPNE1), the anti-GFP antibody revealed a band between 75 kDa and 100 kDa. In the cells transfected with the control plasmid (pEGFP-C1) a band between 25 kDa and 37 kDa was detected,

which corresponds to GFP alone (27 kDa). These data suggest that the GFP-tagged proteins are correctly expressed from the constructed expression plasmids. In agreement with data obtained in fluorescence microscopy, the band corresponding to the fusion CPNE3-GFP is very weak, confirming that this fusion protein is weakly expressed. In addition, the intensity of the bands corresponding to actin has similar intensity, which indicates that the overall amount of proteins is comparable in the different samples.

Together these data demonstrate that the available plasmids are suitable for the expression of GFP-CPNE1 or GFP-CPNE3, and can be used to assess the intracellular localization of CPNE1 and CPNE3 during intoxication by PFTs.

4.2 – Verification of *CPNE1* and *CPNE3* knockout cell lines

To evaluate the putative role of CPNE1 and CPNE3 in the repair of the membrane damage caused by PFTs, the expression of CPNE1 and CPNE3 was abrogated in HeLa cells by CRISPR/Cas9. The two cell lines were previously established and were available in the laboratory. However, to ensure that the genes had been mutated and that the proteins CPNE1 and CPNE3 were not expressed verifications were needed before the use of such cell lines.

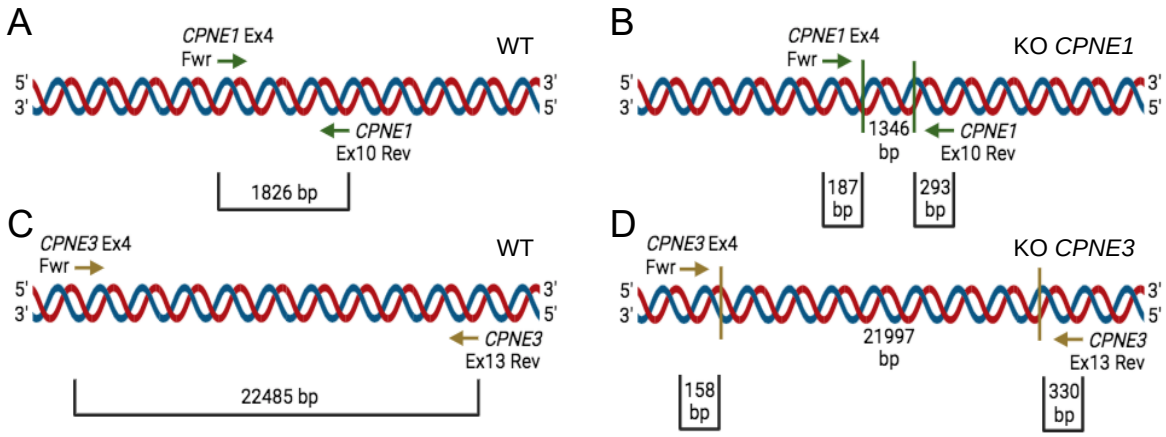

Figure 13: Schematic representation of the gDNA of the different cell lines: WT, KO *CPNE1* and KO *CPNE3*. The primers used for the PCR are indicated (arrows). A: gDNA from WT HeLa cells and size of the expected amplification product using primers for *CPNE1* (control); B: gDNA from KO *CPNE1* HeLa cells and size of the expected amplification product using primers for *CPNE1*. The expected cut sites are indicated by vertical lines; C: gDNA from WT HeLa cells and size of the expected amplification product using primers for *CPNE3* (control); D: gDNA from KO *CPNE3* HeLa cells and size of the expected amplification product using primers for *CPNE3*. The expected cut sites are indicated by vertical lines. Created with BioRender.com

The deletions were first verified by PCR, using primers (Table 3) that flank the cut sites expected to occur in the knockout (KO) cell lines, and the genomic DNA of wild-type (WT) or KO cells. As shown in the scheme (Figure 13), the genomic DNA of KO *CPNE1* cells is expected to lack a fragment of about 1346 bp between the exon 4 and exon 10. In turn, a genomic DNA fragment of 21997 bp between the exon 4 and exon 13 should be missing in the KO *CPNE3* cells. The primers *CPNE1* Forward and *CPNE1* Reverse should thus amplify a fragment of 1.8 kb in the WT genomic DNA and a fragment of 500 bp in the genomic DNA of KO *CPNE1* cells. Primers *CPNE3* Forward and *CPNE3* Reverse should amplify a fragment of 22 kb in the WT and only 500 bp in the KO *CPNE3* genomic DNA.

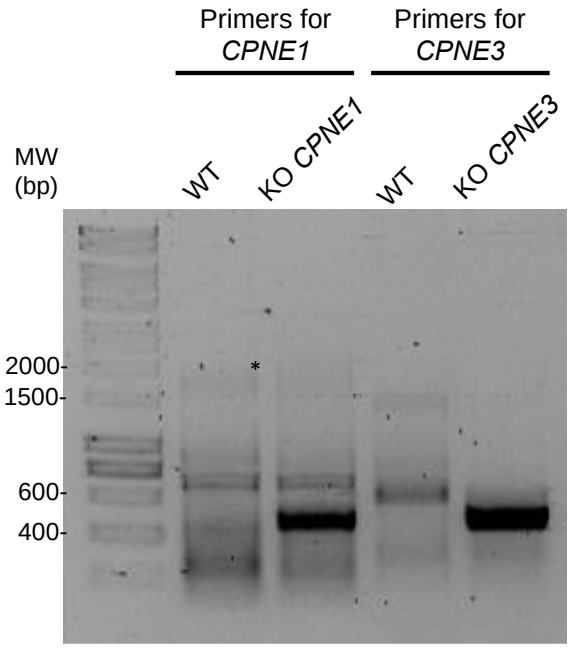

Figure 14: Agarose gel showing the PCR products obtained from the PCR on gDNA of WT, KO *CPNE1* and KO *CPNE3* HeLa cells, using the specific primers flanking the cut sites in *CPNE1* and *CPNE3*.

As shown in the agarose gel (Figure 14), we detected a band of about 500 bp in both KO *CPNE1* and KO *CPNE3* gDNA, which matches the size of the region that we expected to amplify and further indicates that the CRISPR/Cas9 cuts occurred. These bands did not appear in the control samples (gDNA of WT cells). A very faint band of about 1.8 kb (identified by *) was detected using WT gDNA and the primers *CPNE1* Forward and *CPNE1* Reverse, however, the band at 22 kb expected using the primers *CPNE3* Forward and *CPNE3* Reverse could not be detected by the used technique. Overall, the amplification conditions used were not optimal for the amplification in the gDNA template.

To further confirm the sequence of the 500 bp amplification product obtained for KO *CPNE1* and KO *CPNE3* samples, the DNA was purified and sent for sequencing, using the same primers that flank the cuts sites (Table 3). The nucleotide sequence obtained was compared with the original sequence of CPNE1 and CPNE3 available in the databases (Figure 15).

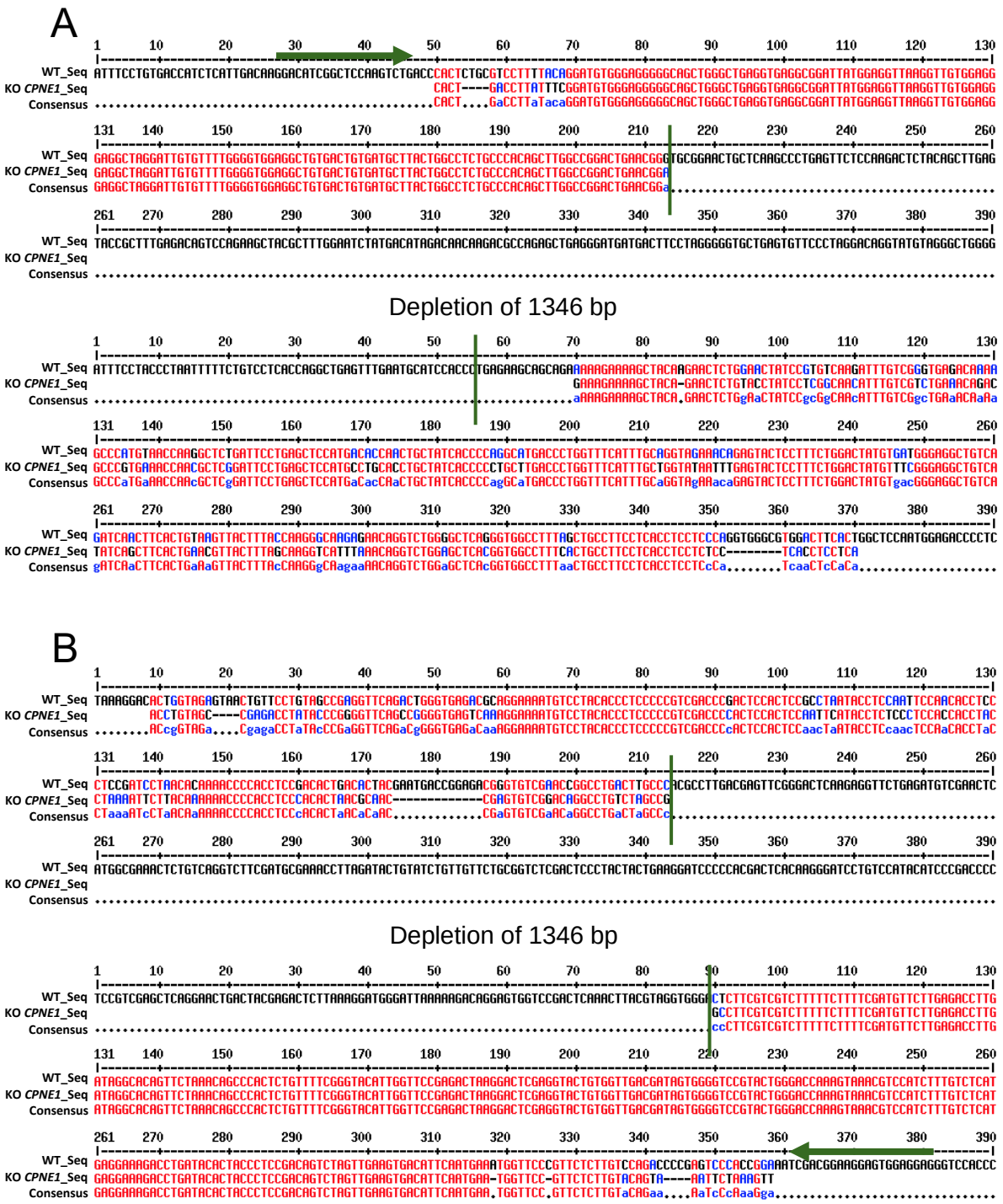

Figure 15: Alignment of the available sequences for *CPNE1* (WT_Seq) with sequence obtained for the 500 bp fragment amplified from gDNA of HeLa cells KO *CPNE1* using primers that flank the cut site. The red color

indicates a high consensus between the sequences, while the blue color indicates a low consensus. Arrows represent the localization of primers used for sequencing, and vertical bars correspond to the expected cut site. A: Alignment of HeLa WT and HeLa KO *CPNE1* sequences, before and after the cut, using *CPNE1* Exon 4 Forward primer; B: Alignment of HeLa WT and HeLa KO *CPNE1* sequences, before and after the cut, using *CPNE1* Exon 10 Reverse primer.

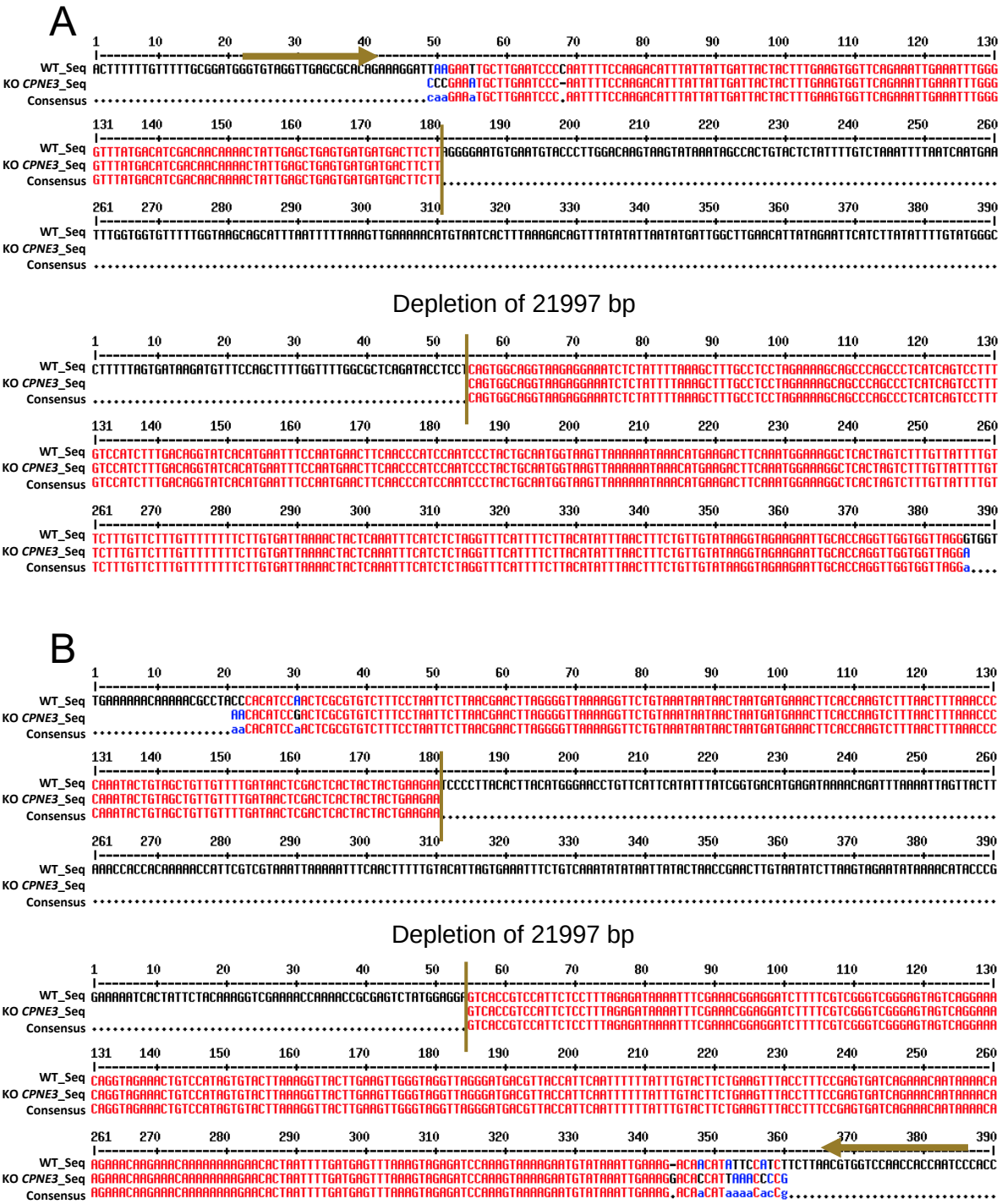

Figure 16: Alignment of the available sequences for *CPNE3* (WT_Seq) with sequence obtained for the 500 bp fragment amplified from gDNA of HeLa cells KO *CPNE3* using primers that flank the cut site. The red color indicates a high consensus between the sequences, while the blue color indicates a low consensus. Arrows

represent the localization of primers used for sequencing, and vertical bars correspond to the expected cut site. A: Alignment of HeLa WT and HeLa KO *CPNE3* sequences, before and after the cut, using *CPNE3* Exon 4 Forward primer; B: Alignment of HeLa WT and HeLa KO *CPNE3* sequences, before and after the cut, using *CPNE3* Exon 10 Reverse primer.

The analysis of the sequences obtained showed that indeed the gDNA of KO *CPNE1* and KO *CPNE3* cells was cut and repaired at the expected sites (Figures 15 and 16). The regions flanking the sites of cut show a 100 % homology with the sequences available in the databases. These data strongly suggest the successful abrogation of the expression of CPNE1 or CPNE3.

To definitively confirm that the KO cells do not express CPNE1 or CPNE3, we performed a western blot on total protein extracts from different cell lines using specific antibodies recognizing CPNE1 or CPNE3 (Figure 17). As a positive control, we used total protein extracts of HeLa cells transfected to express GFP-tagged versions of CPNE1 or CPNE3.

As shown in Figure 17.A, the antibody recognizing CPNE1 revealed different bands: two bands in the extract of cells ectopically expressing GFP-CPNE1, one corresponding to the fusion protein (86 kDa) and the other to the endogenous CPNE1, and one band in the extract of WT HeLa cells which corresponds to CPNE1 (59 kDa). As expected the cells KO for *CPNE1* do not express CPNE1. Curiously, CPNE1 was also not detected in the extracts of cells KO for *CPNE3.* The detection of actin in all the lanes served as positive loading control, ensuring that all the lanes contain a similar amount of protein. This data confirms that KO *CPNE1* cells do not express CPNE1 and are thus useful tools to assess the role of CPNE1 in response to PFTs intoxication. The absence of CPNE1 in the cells KO for *CPNE3* may suggest the existence of a mechanism co-regulating the expression of different copines.

In a similar way, the antibody recognizing CPNE3 also revealed different bands (Figure 17.B). It recognizes both GFP-CPNE3 (87 kDa) and the endogenous CPNE3 (60 kDa) in the protein extracts of cells transfected with pEGFP-*CPNE3*. Also, CPNE3 was detected in the lysates of WT and KO *CPNE1* cells but not in the KO *CPNE3* cells. As above, actin detection ensures an equivalent protein loading in all the lanes. These data indicate that CPNE3 expression was successfully blocked in KO *CPNE3* cells, which may be used to further studies.

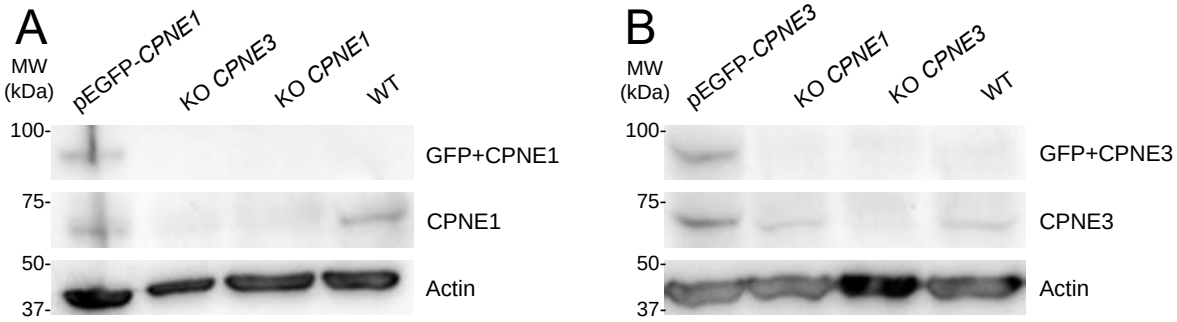

Figure 17: Immunoblots on total protein extracts of WT, KO *CPNE1* and KO *CPNE3* HeLa cells as well as cells overexpressing GFP-CPNE1 or GFP-CPNE3. A: The membrane was incubated with an anti-CPNE1 antibody. Actin signal was used as loading control; B: The membrane was incubated with an anti-CPNE3 antibody. Actin was used as loading control. Molecular weights (MW) of the reference protein ladder are indicated.

Together these observations, lead us to conclude that the abrogation of *CPNE1* and *CPNE3* was successful. From now on, the cells KO *CPNE3* will be considered as Knockout for the two proteins CPNE1 and CPNE3. In agreement with the different validations, we considered that these cell lines can be used to evaluate the role of CPNE1 and CPNE3 during intoxication by bacterial PFTs.

4.3 – Role of CPNE1 and CPNE3 in the cellular response to intoxication by PLY

Having confirmed that the KO cell lines for *CPNE1* and *CPNE3* were indeed impaired in the expression of copines, we used these cells to assess the role of CPNE1 and/or CPNE3 in the cellular response to intoxication by a specific PFT, the PLY. We first evaluate the ability of PLY to permeabilize the KO cell lines in comparison with WT HeLa cells. For that, cells were intoxicated with increasing concentrations of PLY ranging from 0.05 to 0.25 nM and the plasma membrane integrity was assessed by propidium iodide permeability assays under flow cytometry analysis.

We found that for all the cell lines the percentage of PI-positive cells, meaning the percentage of permeabilized cells, increased in a dose-dependent manner with increasing concentrations of PLY (Figure 18). However, the percentage of PI-positive cells remained comparable in the three cell lines for the same PLY concentration, no statistically significant differences were found, suggesting that CPNE1 and CPNE3 are not involved in the initial steps of intoxication (Figure 18).

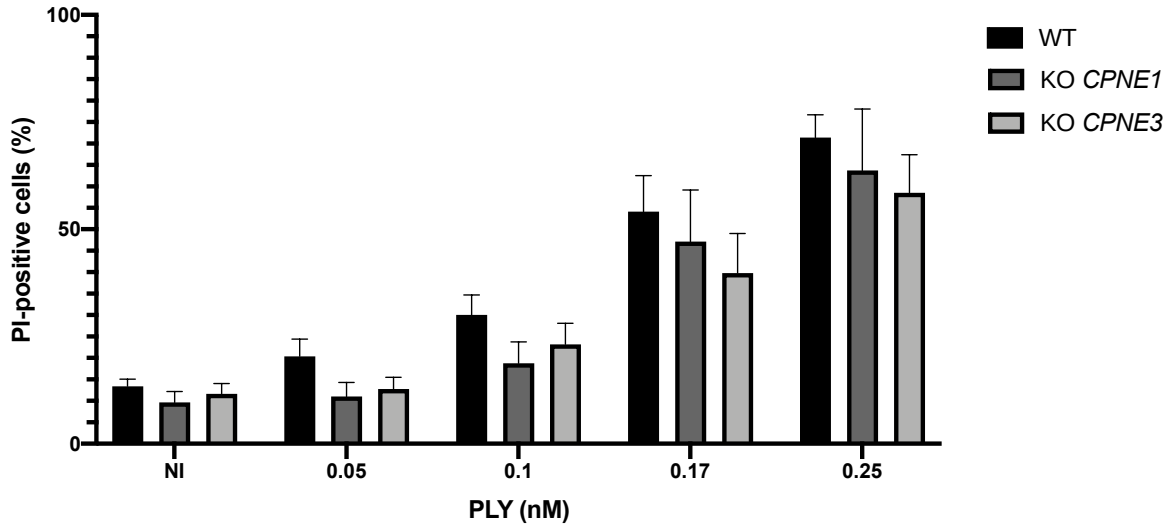

Figure 18: Percentage of PI-positive cells in WT, KO *CPNE1* and KO *CPNE3* HeLa cells left non-intoxicated (NI) or intoxicated with growing concentrations of PLY. Results are the mean ± SEM of 7 experiments. The statistical analysis was performed by Prism using two-way ANOVA analysis with Dunnett's Multiple Comparison.

Importantly, during flow cytometry analysis, we observed that for the samples intoxicated with the higher concentrations of PLY (0.25 nM) the number of events/sec was lower in the KO cell lines than in the control WT HeLa cells. Knowing that we start our experiment with the same number of cells for each cell line and each condition, this decrease in the number of events may indicate that KO cells are overall more sensitive to PLY intoxication and die at concentrations that are sub-lytic for control HeLa cells. If this is true, the dead cells would be washed away during the experiment and would not be accounted in the flow cytometry analysis.

In order to verify our hypothesis, we performed in real-time live cell experiments following PI incorporation along the intoxication by Automated high-throughput Imaging. We designed the experiment in a way that should allowed us to count the total number of cells and the PI-positive cells for each cell line, each PLY concentration and each time point. The reliability of this analysis relies on our ability to define proper fluorescence thresholds using non-intoxicated cells and fully permeabilized cell populations, which we were not able to define due to differences in the background signal and in cell densities. Thus, although very promising, the Automated high-throughput Imaging approach will need further optimization.

Considering our observations from flow cytometry analysis suggesting that at the highest concentration of PLY the KO cell lines die more than the WT HeLa cells, we assessed the ability of cells to repair upon intoxication with 0.17 nM of PLY for 10 min.

Despite at this concentration the KO cells did not show increased permeability as compared to the WT HeLa cells (Figure 18), we hypothesized that if KO cell lines are more susceptible to intoxication it is possible that they show impaired ability to repair and recover PM integrity. To test this hypothesis, KO *CPNE1*, KO *CPNE3* and WT HeLa cells were intoxicated with PLY at 0.17 nM for 10 min, then PLY was washed out and cells were allowed to recover in complete medium for different periods of time ranging from 0 to 2 h. At each time point their permeability to PI was assessed (Figure 19).

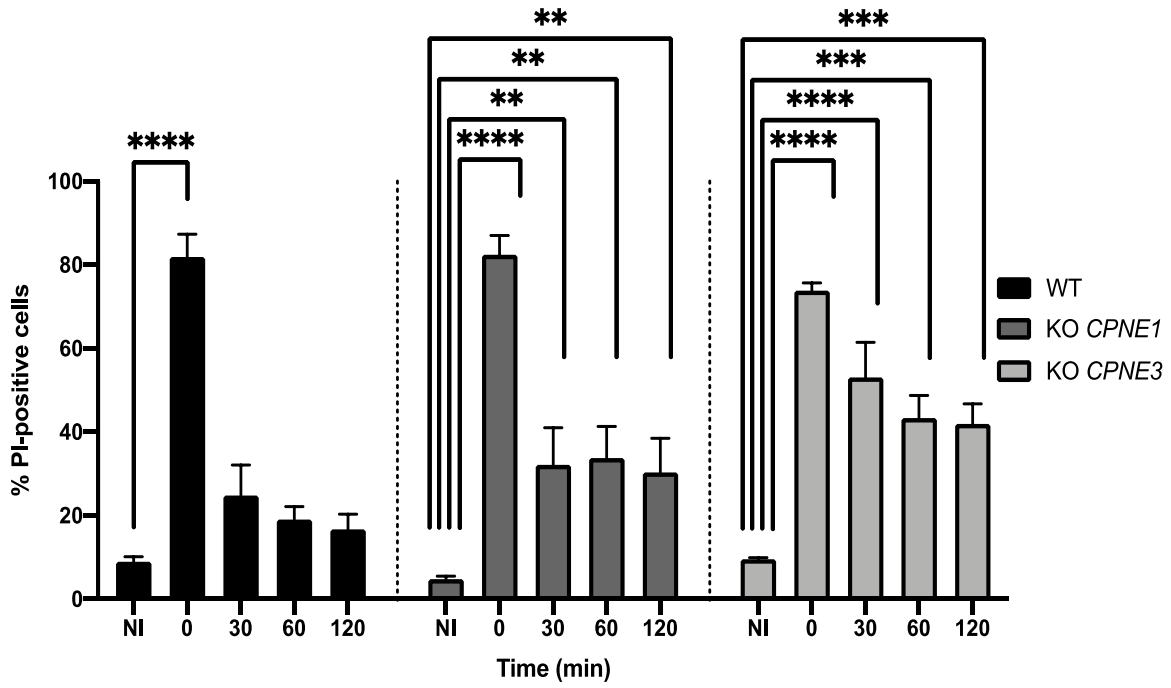

Figure 19: Percentage of PI-positive cells in HeLa WT, KO *CPNE1* and KO *CPNE3* cells left non-intoxicated (NI) or intoxicated with PLY at 0.17 nM for 10 min (T0), and allowed to recover for different time points. Results are the mean ± SEM of 3 experiments. The statistical analysis was performed by Prism using two-way ANOVA analysis with Dunnett's Multiple Comparison.

We found that, as shown in Figure 18, the levels of permeabilization are similar for all the cell lines at T0 (Figure 19). However, while the WT HeLa cells are able to rapidly recover their PM integrity to levels similar to the non-intoxicated (NI) cells, the KO cell lines were not able to recover their PM impermeability even 2 h after PLY washout (Figure 19). These data demonstrated that CPNE1 and CPNE3 are required for the repair of PLY-induced PM damage, as it was suggested by their presence in the extracellular vesicles released by intoxicated cells during repair. Our data also seems to indicate that the impairment in repair is more pronounced in KO *CPNE3* cell line (Figure 19) as the levels of

PI-positive cells are higher than in KO *CPNE1* cells. This may be explained by the fact that these cells lack both CPNE1 and CPNE3 (as shown in Figure 17) and suggests that CPNE1 and CPNE3 may cooperate and compensate each other's function during repair.

4.4 – Intracellular localization of CPNE1 and CPNE3 in cells intoxicated by PLY

As mentioned above, copines are calcium-responding proteins that translocate to the cell cortex and interact with the PM phospholipids in response to increased intracellular calcium concentrations (Creutz *et al*., 1998; Perestenko *et al*., 2010). It is thus expected that their cellular localization changes in response to PM pore formation by PFTs and the consequent calcium influx. To assess this possibility, we used HeLa cells transfected to express the GFP-tagged proteins CPNE1 and CPNE3 (GFP-*CPNE1* and GFP-*CPNE3*). Non-intoxicated and PLY-intoxicated cells were processed for immunofluorescence and observed under confocal microscopy (Figure 20). In addition to CPNE1 and CPNE3 localization, visualized by GFP fluorescence, the cells were immunolabelled for the non-muscle heavy chain of myosin IIA (NMHCIIA), which we previously showed to be recruited to the cortex of the cells, accumulating at specific cortical sites in response to PFTs and playing pivotal roles in repair of the damage (Mesquita *et al*., 2017, Brito *et al*., 2019b). DAPI staining was used to visualize the nuclei.

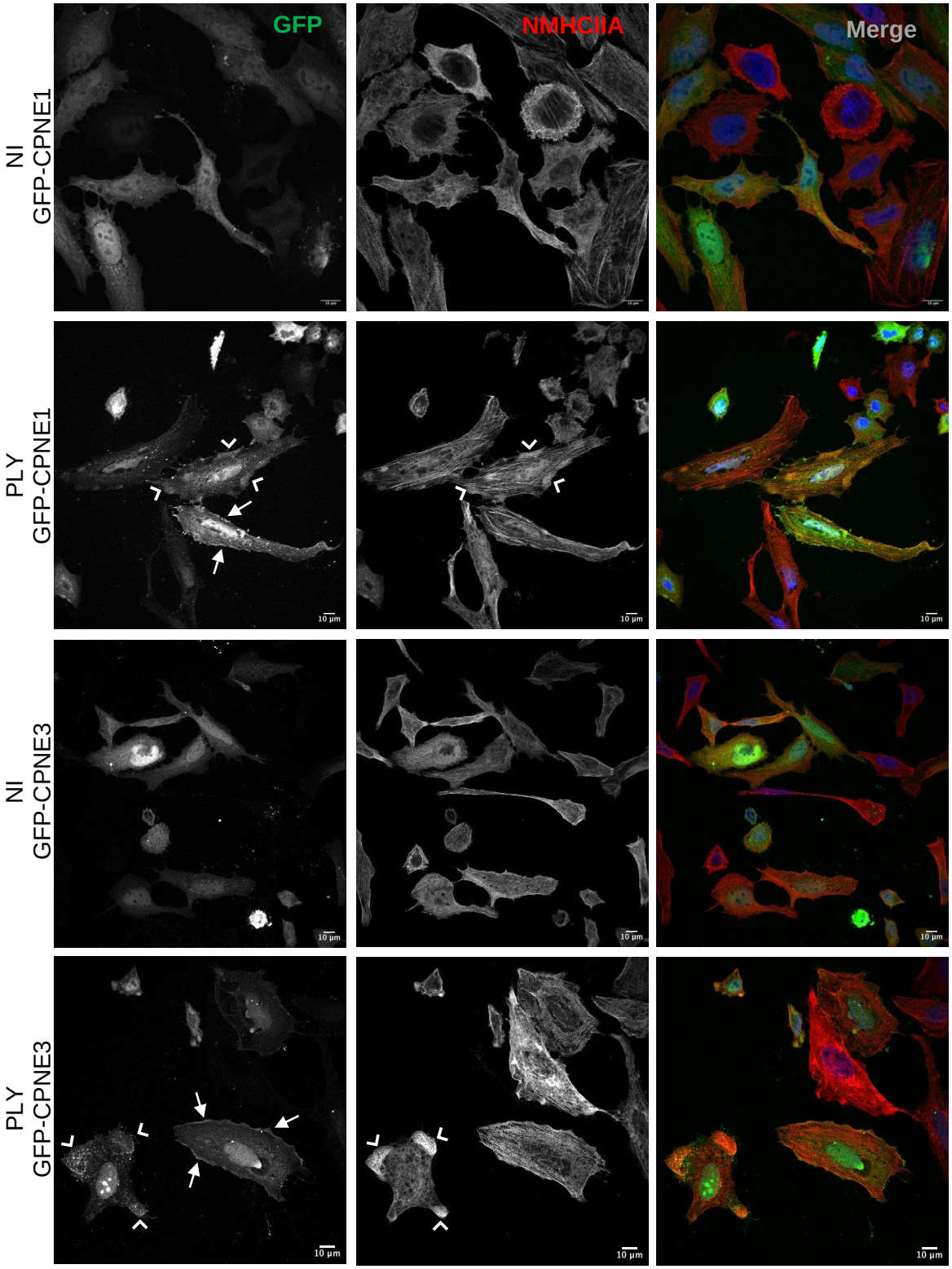

Figure 20: Confocal microscopy images of cells transfected with pEGFP-*CPNE1* or pEGFP-*CPNE3* in non-intoxicated (NI) conditions or intoxicated with PLY at 0.25 nM. The nuclei are detected by DAPI staining (blue). GFP-CPNE1 or GFP-CPNE3 are shown in green. NMHCIIA are immunolabelled in red. Arrows points to CPNE1 or CPNE3 accumulations in the PM. Arrow heads points to CPNE1 or CPNE3 accumulations in NMHCIIA. Scale bar: 10 µm.

As observed above (Figure 11), the GFP signal is uniformly distributed in the cytoplasm of non-intoxicated cells, indicating that the GFP-tagged proteins don't have a particular localization within the cell (Figure 20). In PLY-treated cells the GFP signal, associated to CPNE1 or CPNE3, appears to label the cell PM (arrows, Figure 20), indicating that CPNE1 and CPNE3 translocate to the cortex of the cell in response to intoxication. In addition, we detected the accumulation of CPNE1 and CPNE3 together with NMHCIIA at specific sites (arrow heads, Figure 20). Together, these observations show that CPNE1 and CPNE3 are specifically recruited to the PM in response to PLY and accumulate at specific sites with already identified repair machinery, strongly supporting a role for these proteins in vesicle formation and damage repair, as hypothesized in the beginning of this work.

CHAPTER 5

Conclusions and future perspectives

This work greatly contributed to the ongoing research at the CBBI. As major achievements of the work developed during this Master thesis we may consider: the validation of the tools available in the laboratory to assess in detail the role of CPNE1 and CPNE3 in the response to PFTs; the finding that CPNE1 and CPNE3 are required for efficient PM repair upon PLY intoxication and the data supporting the cellular re-localization of CPNE1 and CPNE3 in response to PLY. Importantly, the data reported here strongly support the first assumption according to which, the proteins enriched in the extracellular vesicles released by intoxicated cells are potentially involved in PM repair and vesicle shedding. In light of the results obtained here, other proteins abundantly detected in the vesicles will be tested for their role in the response to PFTs. Attesting to the high value of the data presented here, part of the results is being included in a manuscript that is in revision for submission.

The data reported here will be further explored and the molecular role of CPNE1 and CPNE3 during the repair of damage caused by PFT will be investigated in detail. In particular, the PI incorporation in real-time experiments will be optimized to pinpoint the difference between the WT and the KO cells. This should reveal the higher susceptibility of KO CPNE1/3 cells to PFTs. The cellular re-localization of CPNE1 and CPNE3 and their accumulation with repair machinery will be followed by time-lapse microscopy in live cells using the GFP-tagged versions of CPNE1 and CPNE3. Finally, following biochemical approaches coupled to mass-spectrometry, the specific interactors of CPNE1 and CPNE3 in response to the intoxication will be identified. The data generated should be of great value in the understanding of the function of copine family of proteins.

Bibliography

Aguilar, J. L., Kulkarni, R., Randis, T. M., Soman, S., Kikuchi, A., Yin, Y., & Ratner, A. J. (2009). Phosphatase-Dependent Regulation of Epithelial Mitogen-Activated Protein Kinase Responses to Toxin-Induced Membrane Pores. *PLoS ONE*, *4*(11). https://doi.org/10.1371/journal.pone.0008076

Alouf, J. E. (2003). Molecular Features of the Cytolytic Pore-forming Bacterial Protein Toxins. *Folia Microbiologica*, *48*(1), 5–16. https://doi.org/10.1007/BF02931271

Alves, S., Pereira, J. M., Mayer, R. L., Gonçalves, A. D. A., Impens, F., Cabanes, D., & Sousa, S. (2022). Cells responding to bacterial pore-forming toxins release extracellular vesicles displaying similar proteomic content. Manuscript in revision.

Ammendolia, D. A., Bement, W. M., & Brumell, J. H. (2021). Plasma membrane integrity: implications for health and disease. *BMC Biology*, *19*(71). https://doi.org/10.1186/s12915-021-00972-y

Anderson, R., & Feldman, C. (2017). Pneumolysin as a potential therapeutic target in severe pneumococcal disease. *Journal of Infection*, *74*(6), 527–544. https://doi.org/10.1016/j.jinf.2017.03.005

Babiychuk, E. B., & Draeger, A. (2015). Defying death: Cellular survival strategies following plasmalemmal injury by bacterial toxins. *Seminars in Cell and Developmental Biology 45*, 39-47. https://doi.org/10.1016/j.semcdb.2015.10.016

Babiychuk, E. B., Monastyrskaya, K., Potez, S., & Draeger, A. (2011). Blebbing confers resistance against cell lysis. *Cell Death and Differentiation*, *18*(1), 80–89. https://doi.org/10.1038/cdd.2010.81

Berry, A. M., Paton, J. C., & Hansman, D. (1992). Effect of insertional inactivation of the genes encoding pneumolysin and autolysin on the virulence of *Streptococcus pneumoniae* type 3. *Microbial Pathogenesis*, *12*, 87–93. https://doi.org/10.1016/0882-4010(92)90111-z

Bischof, L. J., Kao, C. Y., Los, F. C. O., Gonzalez, M. R., Shen, Z., Briggs, S. P., van der Goot, F. G., & Aroian, R. V. (2008). Activation of the Unfolded Protein Response Is Required for Defenses against Bacterial Pore-Forming Toxin *In Vivo*. *PLoS Pathogens*, *4*(10). https://doi.org/10.1371/journal.ppat.1000176

Bischofberger, M., Iacovache, I., & Gisou Van Der Goot, F. (2012). Pathogenic pore-forming proteins: Function and host response. *Cell Host and Microbe*, *12*(3), 266–275. https://doi.org/10.1016/j.chom.2012.08.005

Brito, C., Cabanes, D., Sarmento Mesquita, F., & Sousa, S. (2019a). Mechanisms protecting host cells against bacterial pore-forming toxins. *Cellular and Molecular Life Sciences*, *76*(7), 1319–1339. https://doi.org/10.1007/s00018-018-2992-8

Brito, C., Mesquita, F. S., Bleck, C. K. E., Sellers, J. R., Cabanes, D., & Sousa, S. (2019b). Perfringolysin O-induced plasma membrane pores trigger actomyosin remodeling and endoplasmic reticulum redistribution. *Toxins*, *11*(7). https://doi.org/10.3390/toxins11070419

Cancino-Rodezno, A., Porta, H., Soberón, M., & Bravo, A. (2009). Defense and death responses to pore forming toxins. *Biotechnology and Genetic Engineering Reviews*, *26*(1), 65–82. https://doi.org/10.5661/bger-26-65

Caudell, E. G., Caudell, J. J., Tang, C. H., Yu, T. K., Frederick, M. J., & Grimm, E. A. (2000). Characterization of Human Copine III as a Phosphoprotein with Associated Kinase Activity. *Biochemistry*, *39*(42), 13034–13043. https://doi.org/10.1021/bi001250v

Corbalan-Garcia, S., & Gómez-Fernández, J. C. (2014). Signaling through C2 domains: More than one lipid target. *Biochimica et Biophysica Acta - Biomembranes*, *1838*(6), 1536–1547. https://doi.org/10.1016/j.bbamem.2014.01.008

Cowland, J. B., Carter, D., Bjerregaard, M. D., Johnsen, A. H., Borregaard, N., & Lollike, K. (2003). Tissue expression of copines and isolation of copines I and III from the cytosol of human neutrophils. *Journal of Leukocyte Biology*, *74*(3), 379–388. https://doi.org/10.1189/jlb.0203083

Creutz, C. E., Tomsig, J. L., Snyder, S. L., Gautier, M.-C., Skouri, F., Beisson, J., & Cohen, J. (1998). The Copines, a Novel Class of C2 Domain-containing, Calcium-dependent, Phospholipid-binding Proteins Conserved from *Paramecium* to Humans. *The Journal of Biological Chemistry*, *273*(3), 1393–1402. https://doi.org/10.1074/jbc.273.3.1393

Czuprynski, C. J., & Welch, R. A. (1995). Biological effects of RTX toxins: the possible role of lipopolysaccharide. *Trends in Microbiology*, *3*(12), 480–483. https://doi.org/10.1016/s0966-842x(00)89016-2

Dal Peraro, M., & van der Goot, F. G. (2016). Pore-forming toxins: Ancient, but never really out of fashion. *Nature Reviews Microbiology*, *14*(2), 77–92. https://doi.org/10.1038/nrmicro.2015.3

Damer, C. K., Bayeva, M., Hahn, E. S., Rivera, J., & Socec, C. I. (2005). Copine A, a calcium-dependent membrane-binding protein, transiently localizes to the plasma membrane and intracellular vacuoles in *Dictyostelium*. *BMC Cell Biology*, *6*. https://doi.org/10.1186/1471-2121-6-46

Deamer, D., Dworkin, J. P., Sandford, S. A., Bernstein, M. P., & Allamandola, L. J. (2002). The First Cell Membranes. *Astrobiology*, *2*(4). https://doi.org/10.1089/153110702762470482

Dias, C., & Nylandsted, J. (2021). Plasma membrane integrity in health and disease: significance and therapeutic potential. *Cell Discovery*, *7*(4). https://doi.org/10.1038/s41421-020-00233-2

File Jr, T. M., & Marrie, T. J. (2010). Burden of Community-Acquired Pneumonia in North American Adults. *Postgraduate Medicine*, *122*(2), 130–141. https://doi.org/10.3810/pgm.2010.03.2130

Gilbert, R. J. C. (2002). Review Pore-forming toxins. *Cellular and Molecular Life Sciences*, *59*, 832–844. https://doi.org/10.1007/s00018-002-8471-1

Gilbert, R. J. C., Jiménez, J. L., Chen, S., Tickle, I. J., Rossjohn, J., Parker, M., Andrew, P. W., & Saibil, H. R. (1999). Two Structural Transitions in Membrane Pore Formation by Pneumolysin, the Pore-Forming Toxin of *Streptococcus pneumoniae*. *Cell*, *97*, 647–655. https://doi.org/10.1016/s0092-8674(00)80775-8

González-Juarbe, N., Bradley, K. M., Shenoy, A. T., Gilley, R. P., Reyes, L. F., Hinojosa, C. A., Restrepo, M. I., Dube, P. H., Bergman, M. A., & Orihuela, C. J. (2017). Pore-forming toxin-mediated ion dysregulation leads to death receptor-independent necroptosis of lung epithelial cells during bacterial pneumonia. *Cell Death and Differentiation*, *24*(5), 917–928. https://doi.org/10.1038/cdd.2017.49

González-Juarbe, N., Gilley, R. P., Hinojosa, C. A., Bradley, K. M., Kamei, A., Gao, G., Dube, P. H., Bergman, M. A., & Orihuela, C. J. (2015). Pore-Forming Toxins Induce Macrophage Necroptosis during Acute Bacterial Pneumonia. *PLoS Pathogens*, *11*(12), 1–23. https://doi.org/10.1371/journal.ppat.1005337

Gonzalez, M. R., Bischofberger, M., Pernot, L., van der Goot, F. G., & Frêche, B. (2008). Bacterial pore-forming toxins: The (w)hole story? *Cellular and Molecular Life Sciences*, *65*(3), 493–507. https://doi.org/10.1007/s00018-007-7434-y

Gouaux Eric. (1997). Channel-forming toxins: tales of transformation. *Current Opinion in Structural Biology*, *7*, 566–573. http://biomednet.com/eleeref/O959440XO0700566

Grommes, J., & Soehnlein, O. (2011). Contribution of neutrophils to acute lung injury. *Molecular Medicine*, *17*(3–4), 293–307. https://doi.org/10.2119/molmed.2010.00138

Hamon, M. A., Ribet, D., Stavru, F., & Cossart, P. (2012). Listeriolysin O: The Swiss army knife of *Listeria*. *Trends in Microbiology*, *20*(8), 360–368. https://doi.org/10.1016/j.tim.2012.04.006

Hirst, R. A., Kadioglu, A., O'Callaghan, C., & Andrew, P. W. (2004). The role of pneumolysin in pneumococcal pneumonia and meningitis. *Clinical and Experimental Immunology*, *138*(2), 195–201. https://doi.org/10.1111/j.1365-2249.2004.02611.x

Iacovache, I., van der Goot, F. G., & Pernot, L. (2008). Pore formation: An ancient yet complex form of attack. *Biochimica et Biophysica Acta - Biomembranes*, *1778*(7–8), 1611–1623. https://doi.org/10.1016/j.bbamem.2008.01.026

Ilacqua, A. N., Price, J. E., Graham, B. N., Buccilli, M. J., McKellar, D. R., & Damer, C. K. (2018). Cyclic AMP signaling in *Dictyostelium* promotes the translocation of the copine family of calcium-binding proteins to the plasma membrane. *BMC Cell Biology*, *19*(1), 1–16. https://doi.org/10.1186/s12860-018-0160-5

Jimenez, A. J., & Perez, F. (2017). Plasma membrane repair: the adaptable cell life-insurance. *Current Opinion in Cell Biology*, *47*, 99–107. https://doi.org/10.1016/j.ceb.2017.03.011

Jimenez, A. J., Maiuri, P., Lafaurie-Janvore, J., Divoux, S., Piel, M., & Perez, F. (2014). ESCRT machinery is required for plasma membrane repair. *Science*, *343*(6174). https://doi.org/10.1126/science.1247136

Kafsack, B. F. C., Pena, J. D. O., Coppens, I., Ravindran, S., Boothroyd, J. C., & Carruthers, V. B. (2009). Rapid membrane disruption by a perforin-like protein facilitates parasite exit from host cells. *Science*, *323*(5913), 530–533. https://doi.org/10.1126/science.1165740

Kim, J.-Y., Paton, J. C., Briles, D. E., Rhee, D.-K., & Pyo, S. (2015). *Streptococcus pneumoniae* induces pyroptosis through the regulation of autophagy in murine microglia. *Oncotarget*, *6*(42), 44161–44178. https://doi.org/10.18632/oncotarget.6592

Kloft, N., Busch, T., Neukirch, C., Weis, S., Boukhallouk, F., Bobkiewicz, W., Cibis, I., Bhakdi, S., & Husmann, M. (2009). Pore-forming toxins activate MAPK p38 by causing loss of cellular potassium. *Biochemical and Biophysical Research Communications*, *385*(4), 503–506. https://doi.org/10.1016/j.bbrc.2009.05.121

Kristan, K. Č., Viero, G., Dalla Serra, M., Maček, P., & Anderluh, G. (2009). Molecular mechanism of pore formation by actinoporins. *Toxicon*, *54*(8), 1125–1134. https://doi.org/10.1016/j.toxicon.2009.02.026

Lakey, J. H., Gisou Van Der Goot, F., & Pattus, F. (1994). All in the family: the toxic activity of pore-forming colicins. *Toxicology*, *87*, 85–108. https://doi.org/10.1016/0300-483x(94)90156-2

Linhartová, I., Bumba, L., Mašín, J., Basler, M., Osička, R., Kamanová, J., Procházková, K., Adkins, I., Hejnová-Holubová, J., Sadílková, L., Morová, J., & Šebo, P. (2010). RTX proteins: A highly diverse family secreted by a common mechanism. *FEMS Microbiology Reviews*, *34*(6), 1076–1112. https://doi.org/10.1111/j.1574-6976.2010.00231.x

Loose, M., Hudel, M., Zimmer, K. P., Garcia, E., Hammerschmidt, S., Lucas, R., Chakraborty, T., & Pillich, H. (2015). Pneumococcal Hydrogen Peroxide-Induced Stress Signaling Regulates Inflammatory Genes. *Journal of Infectious Diseases*, *211*(2), 306–316. https://doi.org/10.1093/infdis/jiu428

Los, F. C. O., Randis, T. M., Aroian, R. v., & Ratner, A. J. (2013). Role of Pore-Forming Toxins in Bacterial Infectious Diseases. *Microbiology and Molecular Biology Reviews*, *77*(2), 173–207. https://doi.org/10.1128/mmbr.00052-12

McCain, J. (2013). The MAPK (ERK) Pathway: Investigational Combinations for the Treatment Of BRAF-Mutated Metastatic Melanoma. *Pharmacy and Therapeutics*, *38*(2), 96–108.

McNeil P. L. (1993). Cellular and molecular adaptations to injurious mechanical stress. *Trends in Cell Biology*, *3*, 302–307. https://doi.org/10.1016/0962-8924(93)90012-p

Menestrina, G., Serra, M. D., & Prévost, G. (2001). Mode of action of β-barrel pore-forming toxins of the staphylococcal α-hemolysin family. *Toxicon*, *39*, 1661–1672. https://doi.org/10.1016/s0041-0101(01)00153-2

Mesquita, F. S., Brito, C., Mazon Moya, M. J., Pinheiro, J. C., Mostowy, S., Cabanes, D., & Sousa, S. (2017). Endoplasmic reticulum chaperone Gp96 controls actomyosin dynamics

and protects against pore-forming toxins. *EMBO Reports*, *18*(2), 303–318. https://doi.org/10.15252/embr.201642833

Mitchell, T. J., & Dalziel, C. E. (2014). The biology of pneumolysin. *Sub-Cellular Biochemistry*, *80*, 145–160. https://doi.org/10.1007/978-94-017-8881-6_8

Mondal, A. K., Sreekumar, A., Kundu, N., Kathuria, R., Verma, P., Gandhi, S., & Chattopadhyay, K. (2018). Structural Basis and Functional Implications of the Membrane Pore-Formation Mechanisms of Bacterial Pore-Forming Toxins. *Advances in Experimental Medicine and Biology* (Vol. 1112, pp. 281–291). Springer New York LLC. https://doi.org/10.1007/978-981-13-3065-0_19

Muñoz-Planillo, R., Kuffa, P., Martínez-Colón, G., Smith, B. L., Rajendiran, T. M., & Núñez, G. (2013). K+ Efflux Is the Common Trigger of NLRP3 Inflammasome Activation by Bacterial Toxins and Particulate Matter. *Immunity*, *38*(6), 1142–1153. https://doi.org/10.1016/j.immuni.2013.05.016

Nalefski, E. A., & Falke, J. J. (1996). The C2 domain calcium-binding motif: Structural and functional diversity. *Protein Science*, *5*, 2375–2390. https://doi.org/10.1002/pro.5560051201

Nerlich, A., Mieth, M., Letsiou, E., Fatykhova, D., Zscheppang, K., Imai-Matsushima, A., Meyer, T. F., Paasch, L., Mitchell, T. J., Tönnies, M., Bauer, T. T., Schneider, P., Neudecker, J., Rückert, J. C., Eggeling, S., Schimek, M., Witzenrath, M., Suttorp, N., Hippenstiel, S., & Hocke, A. C. (2018). Pneumolysin induced mitochondrial dysfunction leads to release of mitochondrial DNA. *Scientific Reports*, *8*(1). https://doi.org/10.1038/s41598-017-18468-7

Parker, M. W., & Feil, S. C. (2005). Pore-forming protein toxins: From structure to function. *Progress in Biophysics & Molecular Biology*, *88*(1), 91–142. https://doi.org/10.1016/j.pbiomolbio.2004.01.009

Paton, J. C., Andrew, P. W., Boulnois, G. J., & Timothy Mitchell, K. J. (1993). Molecular Analysis of the Pathogenicity of *Streptococcus Pneumoniae*: The Role of Pneumococcal Proteins. *Annual Review of Microbiology*, *47*, 89–115. https://doi.org/10.1146/annurev.mi.47.100193.000513

Pereira, J. M., Xu, S., Leong, J. M., & Sousa, S. (2022). The Yin and Yang of Pneumolysin During Pneumococcal Infection. *Frontiers in Immunology*, *13*. https://doi.org/10.3389/fimmu.2022.878244

Perestenko, P. V., Pooler, A. M., Noorbakhshnia, M., Gray, A., Bauccio, C., & Jeffrey McIlhinney, R. A. (2010). Copines-1, -2, -3, -6 and -7 show different calcium-dependent intracellular membrane translocation and targeting. *FEBS Journal*, *277*(24), 5174–5189. https://doi.org/10.1111/j.1742-4658.2010.07935.x

Perestenko, P., Watanabe, M., Beusnard-Bee, T., Guna, P., & McIlhinney, J. (2015). The second C2-domain of copine-2, copine-6 and copine-7 is responsible for their calcium-dependent membrane association. *FEBS Journal*, *282*(19), 3722–3736. https://doi.org/10.1111/febs.13370

Porta, H., Cancino-Rodezno, A., Soberón, M., & Bravo, A. (2011). Role of MAPK p38 in the cellular responses to pore-forming toxins. *Peptides*, *32*(3), 601–606. https://doi.org/10.1016/j.peptides.2010.06.012

Potez, S., Luginbühl, M., Monastyrskaya, K., Hostettler, A., Draeger, A., & Babiychuk, E. B. (2011). Tailored Protection against Plasmalemmal Injury by annexins with Different Ca^{2+} Sensitivities. *The Journal of Biological Chemistry*, *286*(20), 17982–17991. https://doi.org/10.1074/jbc.M110.187625

Romero, M., Keyel, M., Shi, G., Bhattacharjee, P., Roth, R., Heuser, J. E., & Keyel, P. A. (2017). Intrinsic repair protects cells from pore-forming toxins by microvesicle shedding. *Cell Death and Differentiation*, *24*(5), 798–808. https://doi.org/10.1038/cdd.2017.11

Rubins, J. B., & Janoff, E. N. (1998). Pneumolysin: A multifunctional pneumococcal virulence factor. *J Lab Clin Med*, *131*, 21–27. https://doi.org/10.1016/s0022-2143(98)90073-7

Sousa, M. V., Richardson, M., Fontes, W., & Morhy, L. (1994). Homology Between the Seed Cytolysin Enterolobin and Bacterial Aerolysins. *Journal of Protein Chemistry*, *13*(8), 659–667. https://doi.org/10.1007/BF01886950

Susin, S. A., Lorenzo, H. K., Zamzami, N., Marzo, I., Snow, B. E., Brothers, G. M., Mangion, J., Jacotot, E., Costantini, P., Loeffler, M., Larochette, N., Goodlett, D. R., Aebersold, R., Siderovski, D. P., Penninger, J. M., & Kroemer, G. (1999). Molecular characterization of mitochondrial apoptosis-inducing factor. *Nature*, *397*, 441–446. https://doi.org/10.1038/17135

Tang, H., Pang, P., Qin, Z., Zhao, Z., Wu, Q., Song, S., & Li, F. (2021). The CPNE Family and Their Role in Cancers. *Frontiers in Genetics*, *12*, 1–7. https://doi.org/10.3389/fgene.2021.689097

Tilley, S. J., Orlova, E. v., Gilbert, R. J. C., Andrew, P. W., & Saibil, H. R. (2005). Structural basis of pore formation by the bacterial toxin pneumolysin. *Cell*, *121*(2), 247–256. https://doi.org/10.1016/j.cell.2005.02.033

Tomita, T., Noguchi, K., Mimuro, H., Ukaji, F., Ito, K., Sugawara-Tomita, N., & Hashimoto, Y. (2004). Pleurotolysin, a novel sphingomyelin-specific two-component cytolysin from the edible mushroom *Pleurotus ostreatus*, assembles into a transmembrane pore complex. *The Journal of Biological Chemistry*, *279*(26), 26975–26982. https://doi.org/10.1074/jbc.M402676200

Tomsig, J. L., & Creutz, C. E. (2000). Biochemical Characterization of Copine: A Ubiquitous Ca^{2+}-Dependent, Phospholipid-Binding Protein. *Biochemistry*, *39*(51), 16163–16175. https://doi.org/10.1021/bi0019949

Tomsig, J. L., & Creutz, C. E. (2002). Copines: a ubiquitous family of Ca^{2+}-dependent phospholipid-binding proteins. *CMLS, Cellular and Molecular Life Sciences*, *59*, 1467–1477. https://doi.org/10.1007/s00018-002-8522-7

Tomsig, J. L., Snyder, S. L., & Creutz, C. E. (2003). Identification of targets for calcium signaling through the copine family of proteins. Characterization of a coiled-coil copine-binding motif.

Journal of Biological Chemistry, *278*(12), 10048–10054. https://doi.org/10.1074/jbc.M212632200

Tomsig, J. L., Sohma, H., & Creutz, C. E. (2004). Calcium-dependent regulation of tumour necrosis factor-α receptor signalling by copine. *Biochemical Society*, *378*, 1089–1094. https://doi.org/10.1042/BJ20031654

Verma, P., & Chattopadhyay, K. (2021). Current Perspective on the Membrane-Damaging Action of Thermostable Direct Hemolysin, an Atypical Bacterial Pore-forming Toxin. *Frontiers in Molecular Biosciences*, *8*, 1–7. https://doi.org/10.3389/fmolb.2021.717147

Verma, P., Gandhi, S., Lata, K., & Chattopadhyay, K. (2021). Pore-forming toxins in infection and immunity. *Biochemical Society Transactions*, *49*(1), 455–465. https://doi.org/10.1042/BST20200836

Voskoboinik, I., Whisstock, J. & Trapani, J (2015). Perforin and granzymes: function, dysfunction and human pathology. *Nat Rev Immunol*, 15, 388–400. https://doi.org/10.1038/nri3839

Weiser, J. N., Ferreira, D. M., & Paton, J. C. (2018). *Streptococcus pneumoniae*: Transmission, colonization and invasion. *Nature Reviews Microbiology*, *16*(6), 355–367. https://doi.org/10.1038/s41579-018-0001-8

Welte, T., Torres, A., & Nathwani, D. (2012). Clinical and economic burden of community-acquired pneumonia among adults in Europe. *Thorax*, *67*(1), 71–79. https://doi.org/10.1136/thx.2009.129502

Whittaker, C. A., & Hynes, R. O. (2002). Distribution and Evolution of von Willebrand/Integrin A domains: Widely Dispersed Domains with Doles in Dell Adhesion and Elsewhere. *Molecular Biology of the Cell*, *13*(10), 3369–3387. https://doi.org/10.1091/mbc.E02-05-0259

Wippel, C., Förtsch, C., Hupp, S., Maier, E., Benz, R., Ma, J., Mitchell, T. J., & Iliev, A. I. (2011). Extracellular Calcium Reduction Strongly Increases the Lytic Capacity of Pneumolysin From Streptococcus pneumoniae in Brain Tissue. *Journal of Infectious Diseases*, *204*(6), 930–936. https://doi.org/10.1093/infdis/jir434

Wolfmeier, H., Radecke, J., Schoenauer, R., Koeffel, R., Babiychuk, V. S., Drücker, P., Hathaway, L. J., Mitchell, T. J., Zuber, B., Draeger, A., & Babiychuk, E. B. (2016). Active release of pneumolysin prepores and pores by mammalian cells undergoing a *Streptococcus pneumoniae* attack. *Biochimica et Biophysica Acta - General Subjects*, 1860(11), 2498–2509. https://doi.org/10.1016/j.bbagen.2016.07.022

Wolfmeier, H., Schoenauer, R., Atanassoff, A. P., Neill, D. R., Kadioglu, A., Draeger, A., & Babiychuk, E. B. (2015). Ca^{2+}-dependent repair of pneumolysin pores: A new paradigm for host cellular defense against bacterial pore-forming toxins. *Biochimica et Biophysica Acta - Molecular Cell Research*, *1853*(9), 2045–2054. https://doi.org/10.1016/j.bbamcr.2014.09.005

Zhou, G., Golden, T., Aragon, I. v., & Honkanen, R. E. (2004). Ser/Thr Protein Phosphatase 5 Inactivates Hypoxia-induced Activation of an Apoptosis Signal-regulating Kinase 1/MKK-4/JNK signaling cascade. *Journal of Biological Chemistry*, *279*(45), 46595–46605. https://doi.org/10.1074/jbc.M408320200